A study of heat transfer from cylinders in turbulent flows by using thermochromic liquid crystals

by

Roland Wiberg

January 2004
Technical Reports from
Royal Institute of Technology
Department of Mechanics/ FaxénLaboratoriet
SE-100 44 Stockholm, Sweden

Typsatt i LaTeX med mekaniks avhandlingsstil.

Akademisk avhandling som med tillstånd av Kungliga Tekniska Högskolan i Stockholm framlägges till offentlig granskning för avläggande av teknologie licentiatexamen fredagen den 23:e Januari 2004 kl 13.15 i hörsal L1, Drottning Kristinas väg 30, Kungliga Tekniska Högskolan, Stockholm.

Universitetsservice US AB, Stockholm 2002

Roland Wiberg 2004 **A study of heat transfer from cylinders in turbulent flows by using thermochromic liquid crystals**

Department of Mechanics/ FaxénLaboratoriet, Royal Institute of Technology
SE-100 44 Stockholm, Sweden

Abstract

In gas quenching, metal parts are rapidly cooled from high temperatures, and the convection heat transfer coefficient distributions are of importance for the hardness and the distortion (the shape nonuniformities) of the quenched parts. Thermochromic liquid crystals (TLC) and a thin foil techniques, were investigated and used for studies of a circular cylinder in axial flows, affected and not affected by upstream flow modifying inserts. Quadratic prisms in cross flows were also studied, a single prism, two prisms arranged in-line, and for four prisms arranged in a square pattern. In this study, particle image velocimetry (PIV) was used for visualization of the flow, giving physical insight to the convection heat transfer data. Further, relations of the type $Nu = CRe^e$ were established. The TLC and thin foil techniques were also used to indicate the dimensions of separated flow regions.

Descriptors: Fluid mechanics, wind-tunnel, turbulence, gas quenching, convection heat transfer, thermochromic liquid crystals, calibration, temperature measurement errors, thin foils, particle image velocimetry, cylinder in axial flow, flow modifying inserts, quadratic prisms in cross flow

Preface

This thesis is a study of 1) experimental methods for surface temperature and convection heat transfer coefficient measurements, and 2) the distributions of Nusselt numbers on a cylinder in axial flows and on prisms in cross flows, at high Reynolds numbers.

Paper 1. Wiberg R. and Lior N., Errors in thermochromic liquid crystal thermometry.

Paper 2. Wiberg R. and Lior N., Heat transfer from a cylinder in axial turbulent flows.

Paper 3. Wiberg R., Stroppiana A. and Lior N., Heat transfer from quadratic prisms in cross flow.

Contents

CHAPTER 1

Introduction

This thesis is a part of a larger FaxénLaboratoriet project about gas quenching of steels. This project is ongoing for a few years, with participation of several Ph.D. and Master students. Some have worked with numerical simulations using different turbulence models etc, and some have done experimental investigations at the Department on Mechanics/ FaxénLaboratoriet KTH, and on-site, using facilities owned by the sponsors.

The present thesis is based on experimental investigations performed in the lab of the Department of Mechanics KTH. The focus of the work is on forced convection heat transfer, and methods on how to measure such convective heat transfer coefficient distributions for bodies and multi-body geometries and configurations common in gas quenching applications. The results from these measurements may be directly applicable for gas quenching purposes, or indirectly for validation of numerical methods for quenching improvements.

Quenching is the rapid cooling of metal parts, such as gears, cylinders, engine axles, bearing rings, etc., which makes the metal hard, by changing its phase structure. Not only must the cooling be rapid, but it is also very important to apply it in a way that will minimize distortions due to internal thermal stresses, a bearing-ring, for example, should remain round also after the quenching process.

In quenching, steel is uniformly heated to ca 800-900 °C, and thereafter rapidly cooled, typically in oils or salts baths. The use of gas as the coolant has several important advantages: the cooled parts do not need to be washed afterwards reducing the use of solvents, the need for ventilation and the risk for fire, the liquid coolants and the solvents pose an environmental problem, the quenched parts retain a very clean surface, and have less distortion Troell & Segerberg (1995) and Minarski *et al.* (2000).

The use of oil and salt solution coolants provides in general higher cooling rates than gas cooling because the cooling is based on boiling, but gas cooling can be improved by using higher gas pressures and velocities, by choosing flows, such as impingement, which provide high heat transfer coefficients, and by the use of gases with better cooling performance such as helium. Another advantage of gas cooling is the possibility of controlling the gas flow during the

cooling process, as well as properly directing it to part locations according to cooling and uniformity need.

A typical facility for gas quenching uses a closed-loop system, where an electric-motor-driven fan moves the gas, which flows a compartment where the hot parts being quenched are placed, then through a water-cooled heat exchanger, and back to the fan inlet. Single chamber Vacuum furnaces and double chamber vacuum furnaces exists, the latter one has initially cold walls which provides higher cooling rates.

Different types of gases may be used for gas quenching. Argon, nitrogen, helium, and hydrogen were compared for that purpose (cf.Minarski *et al.* (2000)). Hydrogen gives the most effective cooling, followed by helium and then nitrogen. Hydrogen becomes flammable and potentially explosive when mixed with oxygen, and helium is expensive if not recycled (Holm & Segerberg (2000)). Commercial vacuum furnaces for gas quenching often use nitrogen or Helium at 10-20 bar and 50-150°C, at a quench zone Inlet velocity of 15-30 m/s [1]. Other parameters which are of importance for gas quench chambers are the uniformity in the inlet gas velocity, and the pressure losses through the quench charge and the system pipes and ducts.

Forced convection heat transfer is usually characterized by the convective heat transfer coefficient, h, defined as,

$$h = \frac{q''}{T - T_\infty} \tag{1.1}$$

where q'' is the convective heat flux, T the surface temperature of the solid which the fluid is exchanging heat, and T_∞ the upstream fluid temperature. This relation is expected to be valid for fluid velocities well below the speed of sound, when $T = T_\infty$ at $q''= 0$.

h is often made dimensionless by dividing it with the reference parameter k/L, which can be seen as a heat transfer coefficient valid for steady state heat conduction through a layer of fluid, with the heat conductivity k, and a thickness equal to the body characteristic dimension L, which thus becomes the Nusselt number Nu,

$$Nu = \frac{hL}{k} \tag{1.2}$$

A large number of metal parts (a charge), may be simultaneously cooled in a gas quench furnace. As an example, the charge may consist of many cylinders in axial or cross flow. In the latter case, each tube-row except the most upstream one is in the wake of other tubes or objects which are upstream of it. To provide the typical magnitudes of some parameters in gas quenching, an example is given below.

[1] Ipsen International GmbH Flutstr. 78 D-47533 Kleve

Nitrogen is filled into a furnace up to $P = 10$ bar at $T_\infty = 80$ °C, and during the cooling the fan gives the gas an inlet velocity of $U_\infty = 15$ m/s. 10 rows of hot solid cylinders at 850 °C made of a low alloy steel with the diameter $D = 30$ mm and arranged in a staggered configuration (at the distances 2×2 D), are introduced into the flow. In the gaps between the cylinders the velocity is higher U_{max}= 30 m/s, which gives a Mach number of M=0.1. For $M << 1$ the flow acts like it is incompressible, the variation in density and temperature etc in the flow are then small.

The Reynolds number Re for the flow over a cylinder is then 4.4×10^5, for which the surface averaged Nusselt number is 1040 and $h = 1000$ W/(m^{2}K) (from Zukauskas & Ziugzda (1985)). Initially, the temperature rise of the gas as it cools this the tube bank can be calculated, using the heat capacitances and the flow rate, to be 80°C, and the effects of the natural convection and the radiation together are calculated to be only a few percent compared to the forced convection heat flux, and decreasing during the subsequent cooling.

For a cooling time t equal to L^2/α (Fourier number $Fo = \alpha t/L^2 = 1$), where L= volume/area for the cylinder, it is estimated that heat has diffused from the core out to the surface, which for this cylinder occur after 7 seconds of cooling. The average cylinder temperature is, at this time, and using a lumped capacitance method, Incropera & De Witt (1990) ch. 5, estimated to be 700°C.

The Biot number for the cylinder is $Bi = hL/k = 0.2$, where k is the heat conductivity of the steel. Bi is a estimate of the temperature differences in the solid, compared to the differences between the cylinder and the gas. Based on this and for $Fo = 1$ the temperature differences in the solid can be estimated to 120°C, decreasing during the cooling period. The time to reach a desired average temperature of 150°C, is estimated using the lumped capacitance method to be 83 seconds. This is then an estimate of the total cooling time for this specific case.

Another issue which is worth mentioning, is the change of the surface temperatures in time during the cooling process, and what possible effect that may have on h. This question may be answered by a simple estimate of the characteristic times involved in the process. The time it takes for the gas to flow from one side to the other of the quenched body above can be estimated to 0.001 s, which is very small compared to the total quenching time estimated to 83 s. The local h for the body, is therfore expected to be equal to h for a body with a temperature constant in time.

Experimental data, for such a cylinder in cross flow, shows that h also varies on the surface ± 50 % and sometimes more around the cylinder perimeter, for tube bundles Zukauskas & Ziugzda (1985), and for a single cylinder at high Re Achenbach (1975). Such local heat transfer coefficients nonuniformities may produce non-uniform hardness and out-of-roundness, and are thus one of the main motivators for the thesis. The geometries studied in this thesis are a

cylinder in axial flows (in paper 2), and single and multiple quadratic cylinders (prisms) in cross flows (in paper 3).

1.1. Some investigations related to gas quenching

Investigations of the gas flows and the resulting convection heat transfer distributions connected to gas hardening problems, have been an question at issue some years for the heat treatment group at FaxénLaboratoriet, involving a few M.S. and Ph.D. students. A review is given below, showing the main contributions from FaxénLaboratoriet and some other publications in this direction so far.

An experimental study was performed using a real gas quenching furnace, in where steel cylinders (400 mm long 30 mm in diameter) were placed in a staggered charge configuration. The cylinders were initially heated to 850°C and then cooled in a flow of nitrogen at 6 bars. During the cooling, the temperatures of the test cylinder were measured using thermocouples, Lind (2001). Noise in the measured data was a problem, but local heat transfer coefficients could be calculated for different temperature levels during the cooling.

The main conclusion from the experiment was that h on the cylinder did not change with the surface temperature, besides for the initial transient fill up of gas into the system, h was in practice constant and independent of $T - T_\infty$. Constant h was also seen from measurements in Nitrogen and Helium and using a cylindrical heat flux sensor, Edenhofer (1996). These results encourage heat transfer coefficient measurements (and simulations), to be performed at lower near ambient temperatures, using wind tunnels etc, and which simplifies and increase the number of methods available for the measurements.

Other investigations also indicates this independence of h for gases. Primarily related to heat exchanger design, numerous measurements of the flow of and the heat transfer coefficients were performed for single cylinders in cross flow, cylinders in staggered configurations, and cylinders in in-line configurations, and at various distances in between, and for convection flows of oil, water and air, Zukauskas (1989) ch. 11 and 13. For all configurations and fluids, and for $Re > 2 \times 10^5$, the surface averaged Nu was successfully expressed as,

$$Nu_f = CRe_f^m Pr_f^n (\frac{Pr_f}{Pr_s})^p \tag{1.3}$$

where m= 0.8, n= 0.4 and p= 0.25, the subscript $_f$ indicates properties evaluated at the fluid temperature, and $_s$ properties evaluated at the wall surface temperature. The characteristic length for Re_f and Nu_f was the diameter of the cylinder. The constant C is 0.023 for a single cylinder, 0.033 for a tube in a inner row of a staggered tube bundle, and a function of the distances between the cylinders for an in-line tube bundle. The exponent n may vary around the

perimeter of the cylinder Zukauskas (1989), and for other flows and geometry's vary in the range n= 0.33-0.43 Incropera & De Witt (1990) ch. 7.

Pr varies strongly with the temperature for water and typically by several orders of magnitudes for oils in the quenching temperature range of interest. For gases (air, nitrogen, helium) at pressures and temperatures relevant for gas quenching, (say 0-1000°C and 1-50 bar), Pr is constant within a few percent, which indicates an independence of Nu on the temperature differences between the surface and the fluid. Equation 1.3 can thus be simplified for gases to

$$Nu_f = CRe_f^m \tag{1.4}$$

Nu_f numbers measured for a specific Re_f for one of these gases are therefore expected to be valid with fair accuracy also for the other gases at the same Re_f.

Another investigation of convective heat transfer from a cylinder in cross flow was performed by the author, using a test cylinder of stainless steel in a wind tunnel, at flows with different velocities and turbulence levels (Wiberg (1999)). In this M.S. thesis a review was given of the different parameters that affect convection heat transfer. Nusselt numbers (Nu), surface pressures, the positions of flow Separation, and the surface shear stress, were measured around the perimeter of the cylinder for Re up to 3×10^5 and TLC was used for the measurement of the surface temperatures. Parts of these results were further published, see Wiberg *et al.* (2000*b*) and in a shorter version, Wiberg *et al.* (2000*a*).

Numerical simulations for a circular cylinder in cross flow were performed, in the FaxénLaboratoriet heat treatment project Lind *et al.* (1998). Three $k-\epsilon$ turbulence models were tested, and one of them the $k-\epsilon$ LSY-CG, produced the best heat transfer coefficients in comparison to available experimental data. Still differences up to 40% was seen in the separated region.

This study was extended by cooperation with the Swedish Institute for Metals Research (SIMR). In this work the h values obtained from the numerical simulation were applied to the surface of a long tube made of bearing ring steel, 32 mm in diameter. The distributions of the relative amounts of the Perlite, Bainite and Martensite phases, and of the hardness, as well as the distortion, were computed using a SIMR code, and were found to be affected by the non-uniform cooling, Thuvander *et al.* (1999).

Further numerical work were performed. A finite length cylinder in axial flows and cylindrical rings were investigated, using different turbulence models. For the cylinder in axial flow which include a large separated and reattached flow region, agreement were found within 30% in comparison to measured heat transfer coefficients (performed by the author, paper 2 in this thesis), using an omega-Reynolds stress model, M. S. thesis by Brandt & Torquist (2003).

Another approach in gas cooling is the use of gas jets, single or Multiple, for cooling many parts distributed in a single layer or individual parts. The cooling rate may be controlled both in space over the surface, and time during the cooling and the cooling rates may be much higher than for uniform flow gas quenching, and higher than for oil quenching, Wunning (1993) and Edenhofer (1999). Different correlations for convective cooling with jets were studied, Ferrari *et al.* (2003). Based on these empirical heat transfer coefficients, simulations of the heat flow and the material structures inside a ring of steel was performed, and an optimal configuration of jet nozzles was suggested.

A parameter of interest in gas quenching is the pressure drop in pipes and ducts and the uniformity in inlet velocities etc. Improvements in these parameters may reduce the power consumption and increase the quenching performance. Such studies have been performed at FaxénLaboratoriet, but are outside the subject of this thesis and are therefore not explained in detail, see paper 1 in the licentiate thesis by Ferrari (2002) and Macchion *et al.* (2003).

Experimental work was performed on convective heat transfer from single and multiple quadratic prisms. This specific geometry was chosen because the flow pattern around them is less sensitive to Re levels, compared for example to that around a circular cylinder, as for example discussed in Zdravkovic (1997). Such data may also serve as a test case in comparisons with numerical simulations.

Heat transfer coefficients around the prisms were measured, using a method in which a solid prism of stainless steel was electrically heated at the core, and surface temperatures were measured using thermochromic liquid crystals (TLC). Based on these data the temperature field inside the prism, and the surface heat flux, were numerically computed, and expressed as local Nu values. Flow velocities around the prisms were also measured using particle image velocimetry (PIV), Wiberg (2000). It was found that this method incurred errors in the measured surface temperatures, which were magnified to larger errors in Nu. A small temperature difference between two closely spaced positions on the surface, is by the heat conduction in the solid connected to large differences in heat flux between these positions. The errors in the temperatures were typically $\pm$ 5 % of the TLC effective range, while the errors in Nu were typically $\pm$ 50%, somewhat reduced after smoothing of the data.

Additional measurements were performed one the quadratic prisms, using the TLC and foil technique and using PIV velocity measurements. Specifically, relations between Nu and different turbulence parameters above the surfaces of separated regions were investigated, in the M.S. thesis by Stroppiana (2001). A close correlation was found between the surface averages of Nu and a turbulence intensity parameter for all geometries studied: a single prism, two prisms in tandem at varying distances, and a prism with a downstream splitter

plate. Local Nu values also showed correlation with the turbulence intensity parameter, for lower average velocities.

1.2. Some methods for the measurement of h

The above-mentioned method for measurement of h, using a body of steel, produced large errors, and a better method was therefore needed. For one class of methods, surface temperatures are measured on a thermally insulated body, and the fluid (or the surface) temperature is subjected to a step or periodic change. The measured transient response in the temperature is introduced into a semi-infinite and one-dimensional solution of the transient heat conduction equation, from which h can be calculated, Camci *et al.* (1993) Yan & Owen (2002) Ireland *et al.* (1999) Von Wolfersdorf *et al.* (1993) Baughn *et al.* (1998) .

The transient temperature change may be introduced by switching valves, insertion of a preheated object, removal of a shield blocking and a upstream thin-wire mesh heater. Advantages of such methods may be the possibility to use them on complex shaped surfaces (with the one-dimensional heat conduction assumption still valid). Disadvantages may be the less controlled surface temperature condition and difficulties to achieve the necessary change in the fluid temperature.

In another method, h is measured in a thermal steady state, while a uniform surface heat flux is applied on a thermally insulated test body. The local h is then directly related to the local surface temperature, which may be measured using TLC, Baughn *et al.* (1985) Hippensteele *et al.* (1985) Gao & Sunden (2001) Praisner *et al.* (2001). The constant heat flux may be delivered from an electrically heated foil, which is thin enough to make the heat conduction parallel in the foil small in comparison to the heat flux to the fluid. Different foils have been tested, gold films on a plastic sheet, carbon impregnated papers, stainless steel. The heat flux may also be applied using radiation from a lamp, Critoph *et al.* (1999).

Advantages of the constant heat flux methods are: 1) large surfaces temperature differences arise, which can thus be measured with a good accuracy, 2) the thermal steady state, which simplifies the measurements, 3) the well defined constant heat flux surface condition. 4) the straightforward calculation of h, from its definition. Disadvantages may be: 1) difficulties to produce a real constant sufficiently uniform heat flux over the entire surface 2) the surfaces can not have complex shapes when using foils.

For the measurements in this thesis, the method using a thin electrically heated foil with TLC was chosen, which for the investigations shown in this thesis gave errors in h typically within 7-8%. For this purpose a new foil

was designed and manufactured [2], which consisted of many closely-spaced thin Inconel strips embedded in a thin plastic sheet,

Inconel has for metals a relatively low thermal conductivity, and its electrical resistance has a weak dependence on the temperature. The foil is described in more detail in papers 2 and 3 in this thesis. Other foils may no be able to produce uniform heat flux, in part caused by the longitudinal Hall effect, which in some cases can make the heat flux 30 % higher at the center of the foil than at the edges, Tarasuk (1983). The uniformity in the delivered heat flux over the surfaces for the foil used here was typically within 1-2 % from its average.

This foil can also be used on surfaces with curved boundaries, such as a cylinder end surface, which is a part of an investigation of a two-diameter long cylinder in axial flows, paper 2 in this thesis.

1.3. A parameter which may affect h

h may depend on the upstream surface temperatures. High upstream surface temperatures heat the fluid, which makes h lower downstream, and low upstream surface temperatures heat the fluid less, which gives a higher h downstream. As an example, the laminar flow over a flat plate having a constant heat flux surface (producing large temperature differences) gives a local h, which is 36 % higher compared to that of a constant temperature surface, Incropera & De Witt (1990) ch. 7. On the other hand, for a turbulent flow over the flat plate, the difference is only 4 %.

In another test, a square prism was used in cross flow for $Re < 5.6 \times 10^4$, no differences were detected in the average Nu (and h) between the case of a constant temperature surface and that of a constant heat flux surface, Igarashi (1985). Here most of the surface was located in separated regions, where the turbulence is high. Therefore, in turbulent flows, the turbulence tends to be more important for h than the upstream temperature history.

Based on this information, and on the fact that most flows in gas quenching are at $Re > 10^5$ and are turbulent, it can be expected that h for such flows are similar within a few percent, i.e. independent of the surface temperature distribution, whether for a constant heat flux surface (with large temperature differences), for an isotherm surface, or for a cooled steel body. Larger differences are expected locally on smooth surfaces, which are facing a low turbulence flow, producing a laminar boundary layer on the surface.

[2] Calesco Foil AB Västeråsvägen 9 S-73040 Kolbäck Sweden

CHAPTER 2

Summary of papers

2.1. Paper 1

This paper investigates experimentally and assesses the errors that may be incurred in the hue-based thermochromic liquid crystal TLC method, and their causes. The errors include response time, hysteresis, aging, surrounding illumination disturbance, direct illumination and viewing angle, illumination light intensity, TLC thickness, digital resolution of the image conversion system, and measurement noise. Some of the main conclusions are that (1) the 3×8 bits digital representation of the red, green and blue TLC color values produces a temperature measurement error of typically 1% of the TLC effective temperature range, (2) an 8-fold variation of the light intensity into the camera produced variations, which were not discernable from the digital resolution error, (3) this temperature depends on the TLC film thickness, (4) thicker films are less susceptible to aging and thickness nonuniformities. Parts of this paper were published Wiberg & Lior (2003*b*).

2.2. Paper 2

Local convection heat transfer coefficients were measured on a two-diameter long cylinder in axial flows of air, at Reynolds numbers of $8.9\times10^4 < Re < 6.17\times10^5$ (9 to 63 ms$^-$1), using thermochromic liquid crystals (TLC) and a electrically heated foil consisting of thin metal bands. The flow in front of the cylinder was modified by the use of a turbulence generating grid, and by inserts, circular discs of two sizes, in front of the cylinder. These create a major change in the local convection heat transfer coefficient distribution on the cylinder. Increase of the turbulence intensity from $Tu < 0.1\%$ to 6.7 % at the same Re, increased the average calculated Nusselt number Nu over the cylinder by 25%, and decreased the Nu non-uniformity (σ_{Nu} and σ_{max}) by 30% and 12% respectively. One of the flow modification inserts reduced σ_{Nu} by 25%. The position of flow reattachment was measured using tufts, and the envelope of the flow separation region was successfully visualized by a specially TLC-based heated flat plate mounted in the flow above the cylinder. Correlation's between the Nu and Re in the form $Nu = CRe^e$ were established and presented for the average Nu on the three different cylinder surfaces, and the variation of

the local exponent e was shown along the cylinder. Parts of this paper were published Wiberg & Lior (2003*a*).

2.3. Paper 3

Experimental investigations on the local and average heat transfer from a square prism, with an edge facing the flow, and from two prisms arranged in-line at different distances, and from four prisms arranged in a square, were carried out in cross flows of air at Reynolds numbers $2.9\times10^4 < Re < 1.39\times10^5$. Thermochromic liquid crystals (TLC) and thin foils, were used for these measurements and particle image velocimetry (PIV) was used for flow velocity measurements. A splitter plate behind the single prism killed the vortex shedding and halved the average Nusselt number Nu on the downstream side. For the two prisms arranged in-line, Nu showed three main different distributions appearing in three different intervals of distance, and the flow was found to be unstable and intermittently switching, in the interval 5.83 to 6.67 side lengths between the prisms. The largest values in Nu appeared for distances 1.66 to 2.00 side lengths apart. The experimental work on the convective heat transfer was carried out by Roland Wiberg and Alberto Stroppiana in equal parts, while the PIV measurements were carried out by Alberto Stroppiana and in part evaluated by the author.

CHAPTER 3

Conclusions

This thesis is a part of a project for improving gas quenching, and describes several advances in the state of the art of measurement methods, knowledge of convective heat transfer from single and multiple bodies in cross- and axial-turbulent flows, and the fluid dynamics that dominates this heat transfer. The primary new findings relative to the state of the art are:

Thermochromic liquid crystals (TLC) and thin foil techniques, were used together with digital image computer processing for the measurements of the convective heat transfer. Different parameters, which affects the TLC measurements were found in the literature, and other parameters were found and quantified by experiments, especially the aging of the TLC and its relation to the TLC film thickness.

For the measurements of the convective heat transfer a thin heating foil was designed, which was shown to produce a constant heat flux over the surface investigated within 1-2%. The TLC measured temperatures had errors typically within $< \pm 5\%$, of its effective temperature range. The errors in the measured h and Nu were then estimated within $\pm$ 7-8 %.

Nu was measured on a two-diameter long cylinder in axial flows of air, at Reynolds numbers of $8.9{\times}10^4 < Re < 6.17{\times}10^5$ (9 to 63 ms$^-$1). In quenching the uniformity in h (and Nu) is of importance and some attempts to modify the distribution were made by the use of a turbulence generating grid, and by inserts, circular discs of two sizes, in front of the cylinder. In this comparison, the grid generated turbulence gave the smallest non-uniformity and an increased Nu.

In purpose to visualize the separated flow region above the cylinder, the TLC and the foil techniques were used on a thin plate inserted parallel with the flow. A maximum convective heat transfer track appeared on the plate, which was found to agree well with the dividing stream line, measured for a similar axial flow.

Nu was measured on a single square prism, with and without a downstream splitter plate eliminating the vortex shedding, and for two prisms arranged in-line at different distances apart, and for four prisms arranged in a square pattern, for $2.9 \times 10^4 < Re < 1.39 \times 10^5$ at low upstream Tu. Except for the single square prism in cross flow, such data are not found in the literature,

while data exists for circular cylinders in similar configurations. In addition, PIV measured velocities were shown and were qualitatively related to Nu for these flows.

Nu measured for a specific Re on a bluff body with a constant heat flux surface, as was used here, and in highly turbulent flows, is expected to be valid with a fair accuracy also for a body, in the gas quenching process, which is of the same shape and is located in the same type of upstream flow (turbulence levels, etc), and independent of $(T - T_\infty)$, type of gas used, gas pressure, and the temperature distribution on the body.

CHAPTER 4

Acknowledgments

This work was partially supported by AGA AB (now Linde Gas), SKF Engineering and Research Center, B.V., the Volvo Research Foundation, and Volvo Personvagnar Komponenter AB and Ipsen International GmbH. I want to thank Prof. Fritz Bark the head of FaxenLaboratoriet. Further I want to thank Prof. Noam Lior at the University of Pennsylvania U.S.A., my research supervisor and the head of the heat treatment project at FaxenLaboratoriet. I also want to thank Dr. Barbro M. Klingmann for her cooperation in the work, especially in paper 3. Marcus Gällstedt and Ulf Landen is acknowledged for their valuable help with the experimental equipment. Ulf Andersson at Calesco foil AB is acknowledged for his constructive cooperation. I also appreciates the the colleagues with whom I played indoor bandy, and other people at the Department of Mechanics who participated in other activities, coffee breaks, sailing etc.

References

Achenbach, E. 1975 Total and local heat transfer from a smooth circular cylinder in cross-flow at high reynolds number. *Int. J. of Heat and Mass Transfer* **18**, 1387–1396.

Baughn, J., Mayhew, J. & et al., A. M. 1998 A periodic transient method using liquid crystals for the measurement of local heat transfer coefficients. *J. of Heat Transfer* **120** (3), 772–777.

Baughn, J., Takahashi, R. & Hoffman, M. e. a. 1985 Local heat-transfer measurements using an electrically heated thin gold-coated plastic sheet. *J. of Heat Transfer* **107** (4), 953–959.

Brandt, M. K. & Torquist, T. 2003 To be finished. Master thesis. Dept. of mechanics/FaxénLaboratoriet, KTH.

Camci, C., Kim, K., Hippensteele, S. A. & Poinsatte, P. E. 1993 Evaluation of a hue based transient liquid crystal method for high-resolution mapping of convective heat transfer on curved surfaces. *J. of Heat Transfer* **115**, 311–318.

Critoph, R., Holland, M. & Fisher, M. 1999 Comparison of steady state and transient methods for measurement of local heat transfer in plate fin-tube heat exchangers using liquid crystal thermography with radiant heating. *Int. J. of Heat and Mass Transfer* **42** (1), 1–12.

Edenhofer, B. 1996 Steuerung der hochdrucksgasabschreckung mittels wärmestromsensor. *HTM* **51** (5), 314–318.

Edenhofer, B. 1999 An overview of advances in atmosphere and vacuum heat treatment. *Heat treatment of metals* **1**, 1–5.

Ferrari, J. 2002 Studies of flow and heat transfer in gas quenching; quench chambers, impingement cooled bodies, and inverse solutions. Licentiate Thesis ISRN KTH/MEK/TR–02/02-SE. Department of mechanics/ FaxénLaboratoriet, KTH.

Ferrari, J., Lior, N. & Slycke, J. 2003 An evaluation of gas quenching of steel rings by multiple-jet impingement. *J. Materials Processing Technol.* **136**, 190–201.

Gao, X. & Sunden, B. 2001 Heat transfer distribution in rectangular ducts with v-shaped ribs. *Heat and Mass Transfer* **37** (4-5), 315–320.

Hippensteele, S., Russell, L. & Torres, F. 1985 Local heat-transfer measurements on a large scale-model turbine blade airfoil using a composite of a heater element and liquid-crystals. *J. eng. gas turb. power* **107** (4), 953–960.

Holm, T. & Segerberg, S. 2000 Helium recovery and cleaning for high-pressure gas quenching connected to an atmosphere furnace. *Heat treatment of metals* **1**, 9–12.

Igarashi, T. 1985 Heat transfer from a square prism to an air stream. *Int. J. of Heat and Mass Transfer* **28** (1), 175–181.

Incropera, F. P. & De Witt, D. P. 1990 *Fundamentals of heat and mass transfer, third ed.*. Wiley, New York.

Ireland, P., Neely, A. & Gillespie, D. e. a. 1999 Turbulent heat transfer measurements using liquid crystals. *Int. J. of Heat and Fluid Flow* **20** (4), 355–367.

Lind, M. 2001 Report from a quench tank experiment. Not publicated report. Dept. of mechanics/FaxénLaboratoriet, KTH.

Lind, M., Lior, N., Alavyoon, F. & Bark, F. 1998 Flows effects and modeling in gas-cooled quenching. In *Proc. Heat Transfer 1998, 11th International Heat Transfer Conference, Kyongju, Korea*, , vol. 3, pp. 171–176.

Macchion, O., Lior, N. & Rizzi, A. 2003 Computational study ofvelocity distribution and pressure drop for designing gas quenchchamber and furnace ducts. In *Proc. International Conference on Advances in Materials and Processing Technology, AMPT 2003, Dublin, Ireland*, , vol. 1, pp. 155–158.

Minarski, P., Preisser, F. & Wilfried, R. Z. 2000 Quenching steel parts in 20-bar helium. *Advanced materials and processes, April* pp. 23–26.

Praisner, T., Sabatino, D. & Smith, C. 2001 Simultaneously combined liquid crystal surface heat transfer and piv flow-field measurements. *Experiments in Fluids* **30** (1), 1–10.

Stroppiana, A. 2001 Experimental investigation of velocity field and heat transfer in separated forced convection past a square cylinder in cross flow. Master Thesis, Department of mechanics/ FaxénLaboratoriet, KTH Printed at: Politechnico di Milano, Facolta de Ingegneria, Corso di Laurea in Ingegneria Aerospaziale, Tesi di Laurea, Matt. N. 629499, Anno Accademico 2000-2001.

Tarasuk, J. D. 1983 Temperature distribution in an electrically heated wide metallic foil. *J. of Heat Transfer* **105** (1), 210–212.

Thuvander, A., Melander, A., Lind, M., Lior, N. & Bark, F. 1999 Prediction of convective heat transfer coefficients and their effects on distortion and mechanical properties of cylindrical steel bodies quenched by gas cooling. In *paper AJTE99-6289 in 5th ASME/JSME Joint Thermal Engineering Conference, San Diego*, pp. 171–176.

Troell, E. & Segerberg, S. 1995 Kylning i kväve och helium under högt tryck. Technical report IVF-skrift 95845. The swedish Institute of Production Engineering Research (IVF).

Von Wolfersdorf, J., Hoecker, R. & Sattelmayer, T. 1993 A hybrid transient step-heating heat-transfer measurement technique using heater foils and liquid-crystal thermography. *J. of Heat Transfer* **115** (2), 319–324.

Wiberg, R. 1999 Experimental study of the heat transfer from a cylinder in a cross

flow, using thermochromic liquid crystals. Master Thesis 1999:08. Department of mechanics/ FaxénLaboratoriet, KTH.

Wiberg, R. 2000 Heat flux and velocity measurements on and around a single quadratic cylinder and using groups of quadratic cylinders in the cross flow of air. Not publicated https://www2.mech.kth.se/liorweb/roland/. Dept. of mechanics/FaxénLaboratoriet, KTH.

Wiberg, R. & Lior, N. 2003*a* Convection heat transfer coefficients for axial flow gas quenching of a cylinder. In *Proceedings of the Fourth International Conference on Quenching and Control of Distortion, Beijing, China*. Chinese Heat Treatment Soceity (CHTS).

Wiberg, R. & Lior, N. 2003*b* Error causes and magnitudes in thermochromic liquid crystals thermometry, paper imece2003-42101. In *IMECE'03, 2003 ASME International Mechanical Engineering Congress & Exposition Washington, D.C., USA*, pp. 15–21.

Wiberg, R., Muhammad-Klingmann, B., Ferrari, J. & Lior, N. 2000*a* Thermochromic coatings help characterize gas quenching. *ASM International Heat Treating Progress* **158** (4), 37–40.

Wiberg, R., Muhammad-Klingmann, B., Ferrari, J. & Lior, N. 2000*b* Use of thermochromic coatings for the experimental determination of the distribution of heat transfer coefficients in gas-cooled quenching. In *Proc. 5th ASM Heat Transfer and Surface Eng. Conf. in Europe., Gothenburg, Sweden*, pp. 275–286.

Wunning, J. 1993 Einzelhrtung von serientielen in gasdusenformen. *HTM* **48** (3), 199–204.

Yan, Y. & Owen, J. 2002 Uncertainties in transient heat transfer measurements with liquid crystal. *Int. J. of Heat and Fluid Flow* **23** (1), 29–35.

Zdravkovic, M. M., ed. 1997 *Flow around circular cylinders, vol. 1 Fundamentals*. Oxford science publications, Oxford University Press Inc.: Oxford.

Zukauskas, A. 1989 *High-performance single-phase heat exchangers*. Hemisphere Pub., New York.

Zukauskas, A. & Ziugzda, J., ed. 1985 *Heat Transfer of a cylinder in Crossflow*. Springer- Verlag, Berlin.

P1

Paper 1

Errors in thermochromic liquid crystal thermometry

By Roland Wiberg* and Noam Lior**

*FaxénLaboratoriet, Dept. of Mechanics, KTH, SE-100 44 Stockholm, Sweden
Email: roland@mech.kth.se
**Dept. of Mechanical Engineering and Applied Mechanics, University of Pennsylvania, Philadelphia, PA 19104-6315, U.S.A.

Submitted for publication

This paper investigates experimentally and assesses the errors that may be incurred in the hue-based thermochromic liquid crystal TLC method, and their causes. The errors include response time, hysteresis, aging, surrounding illumination disturbance, direct illumination and viewing angle, illumination light intensity, TLC thickness, digital resolution of the image conversion system, and measurement noise. Some of the main conclusions are that (1) the 3×8 bits digital representation of the red, green and blue TLC color values produces a temperature measurement error of typically 1% of the TLC effective temperature range, (2) an 8-fold variation of the light intensity into the camera produced variations, which were not discernable from the digital resolution error, (3) this temperature depends on the TLC film thickness, (4) thicker films are less susceptible to aging and thickness nonuniformities.

Key Words: Temperature measurement, Thermochromic liquid crystals, Temperature measurement errors.

1. Nomenclature

TLC Thermochromic Liquid Crystals.
ϕ incidence angle, degrees
T temperature, °C
R quantity of red colored light, dimensionless
G quantity of green colored light, dimensionless
B quantity of blue colored light, dimensionless
H hue, dimensionless
I total quantity of light, J
n aperture number of the camera
ΔT difference in temperature, $°C$

Subscripts
av average

2. Introduction

2.1. *The TLC method*

In our ongoing work to adapt and develop the thermochromic liquid crystal TLC method (used widely for the non-invasive visualization and measurement of surface temperature fields) for measuring surface heat transfer coefficient fields in complex high- speed turbulent flows with separation (application to gas quenching, Wiberg *et al.* (2000), we have used a hue based method for the measurements. Hue is a color variable and for the reflected light from a TLC, it increase typically with the TLC temperature. In this paper we analyze and measure the major sources of error and recommend ways for their reduction.

One of the many advantages of the TLC technique is that the reflected light from the TLC-s is within the visible wavelength, allowing viewing and photography of the objects using commercial digital color video cameras through visible transparent fluids and solid materials. TLC's show temperature-dependent colors by selectively reflecting incident white light, and the best color play performance appear when they are applied as a thin film on a light-absorbing black background.

The reflected wavelength is typically decreasing with rising temperatures. At temperatures lower than its starting point it is colorless, and with rising temperatures the TLC turns red, orange, yellow, green, blue and finally violet, sequentially, before turning colorless again. The color changes are in principle reversible, and on cooling the color change sequence is reversed.

The reflected light from a film of TLC is circularly polarized, because of the twisted structure of the molecule layers. Crossed polarizers in front of the light source and in front of the camera objective, can therefore reduce the direct reflected non-polarized light from the TLC's, Fergason (1968).

In this study the TLC colors are obviously affected by many parameters beside temperature; such as illumination, viewing incidence angles, TLC film thickness, and by the measurement and image processing method. The TLC's used here are micro-encapsulated in thin protective spheres in sizes down to a few micro meter. Together with a binder and mixed with water the micro spheres form a stabilized aqueous slurry. Techniques on how to apply the TLC as a sprayed film and on how to achieve uniform films are described, Farina & Hacker (1994). Pre- manufactured plastic sheets coated with black primary color and TLC are available, Hallcrest[1].

A monochrome camera and 18 optical band pass filters active within different wave lengths were used for TLC temperature measurements, Akino *et al.* (1989). A CCD digital camera, such as the one used here, typically uses only three band pass filters (or other selective device), which transmit Red, Green and Blue light to the sensors. Each pixel in an image then contains the information about the R , G, and B intensities. It is noteworthy though that despite this reduced information about the light, combinations of R , G, and B can form any visible color.

The quantity hue H can be calculated using the R , G and B magnitudes, and it increases when the dominant color transits from R , to G and then to B. This property of hue and its independence of the light intensity levels, makes it suitable for temperature measurements using TLC. Three somewhat different versions of hue were investigated, Hay & Hollingsworth (1996) one of these produced less errors in the temperature reading. The recommended version of hue was found similar to the Matlab^{TM} function $rgb2hsv$, Baughn *et al.* (1999). Matlab5.2.1^{TM} [2] for Macintosh was used in this report, that calculates hue using Eqs. (1- 4),

for $R = \max(R\ ,G,B)$ and $G < B$,

$$H = \frac{1}{6}\left(\frac{G-B}{R-\min(RGB)}\right) + 1 \tag{1}$$

for $R = \max(R\ ,G,B)$ and $G > B$,

$$H = \frac{1}{6}\left(\frac{G-B}{R-\min(RGB)}\right) \tag{2}$$

for $G = \max(R\ ,G,B)$,

$$H = \frac{1}{6}\left(2 + \frac{B-R}{G-\min(RGB)}\right) \tag{3}$$

for $B = \max(R\ ,G,B)$,

[1]Hallcrest 20 Downing Road, West Meadows Industrial Estate, Derby, UK, DE21 6HA.
[2]The MathWorks, 3 Apple Hill Drive, Natick, MA 01760-2098

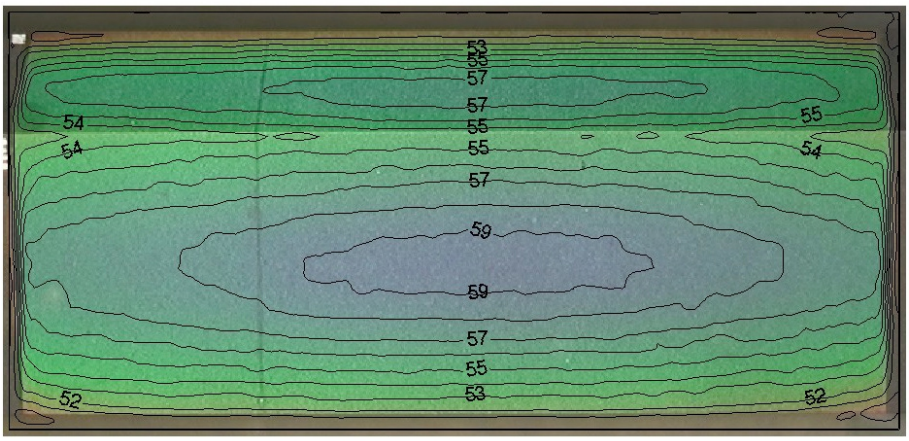

FIGURE 1. Example of measured temperatures (°C), using the TLC technique, on a heated quadratic prism of metal cooled by a cross flow of air.

$$H = \frac{1}{6}(4 + \frac{R - G}{B - \min(RGB)}) \tag{4}$$

An example of a temperature measurement using the present TLC technique is shown in Fig. 1. Isotherms were plotted on the original color image from which the temperatures were evaluated. Measured on an internally heated quadratic prism of metal, in the cross flow of air.

2.2. *Parameters affecting TLC measurements: a brief survey of existing work*

2.2.1. *Response Time*

Cholesteric liquid crystals used for thermal mapping have a response time of about 100 ms, which is the time required for the molecules to attain a new configuration after a change in its temperature, Fergason (1968). The response time for an encapsulated chiral nematic TLC was investigated, Ireland & Jones (1987) , Ireland & Jones (2000). A TLC film ca 10 μm thick, was applied to a blackened metal foil, which was electrically heated. A white light source was used and the reflected light from the TLC was measured using a photodiod detector and the response time was found to be a few milliseconds.

2.2.2. *Hysteresis*

The color response of TLC is known to be different on cooling and heating, the differences can be significantly reduced if the heating and cooling are kept below the upper temperature limit of the specific TLC. Furthermore, the TLC

is found to reset when it is cooled below the start temperature for the color play, Baughn *et al.* (1999) , Birrell & Eaton (1998). On the other hand it was found that a TLC (24.5 to 30°C) was permanently altered after the temperature was increased to 42°C, causing a change of 13% of the TLC hue bandwidth, Sabatino *et al.* (2000). Possibly related, is the change of the TLC with time, the aging, especially at higher temperatures, which is one of the sources of error pursued further in this paper.

2.2.3. *Light disturbances*

Uncontrolled light sources and possible reflections from surfaces in the view field of the TLC measurement target may cause errors in the measured temperatures. The intensity of the light used to illuminate the TLC should obviously be much stronger than the light incident onto the TLC from other non-controlled sources.

Reflections can be minimized by shielding the primary light to fall on the TLC surface only, and by making all the surrounding surfaces non-reflective. Experiments have shown that reflections and spurious light sources caused an error of up to 17% of the effective temperature measurement range, (a range in which hue is monotonically increasing), Farina & Hacker (1994). Tungsten-halogen lamps were recommended, Chan *et al.* (2001).

2.2.4. *Illumination and viewing incidence angles*

The reading of the TLC colors was found to be dependent on the angles between the light source and the TLC surface, and between the camera and the TLC surface. If the illumination and viewing are on the same line (on-axis), the angle effect was minimized. Amounting to a measurement error of only a few percent of the effective hue range for angles 0 to 70 degrees, while off-axis light and viewing could result in much higher errors, Herold & Wiegel (1980), Farina & Hacker (1994), Chan *et al.* (2001), Camci *et al.* (1992) , Behle *et al.* (1996).

2.2.5. *Illumination intensity*

The light intensity entering a CCD camera may have an influence on the colors and hue, which may be influenced from the "gamma correction" of the camera, which reduce the signal for higher light intensities. The light intensity was reduced by 75% giving a change in hue of 4% for an optimal choice of the white balance camera setting, Camci *et al.* (1992) , Behle *et al.* (1996). (The white balance is usually used to compensate the colors for a non-white light source.) This is one of the sources of error pursued further in this paper.

2.2.6. *TLC film thickness*

The thickness of a TLC film is known to have an influence on the reflected colors, and film thickness nonuniformity will thus also cause errors in the measured

temperatures. In a calculation on the light transmitted through a cholesteric TLC and on its film thickness it was concluded that a film thickness of 20 μm was sufficient, Fergason (1968). An TLC of type R30C5W was applied in three different films 14, 23 and 34 μm thick and the maximal difference found for these films at a constant hue, was 2°C, which was 14% of the used TLC temperature range 32 to 44°C, while the difference was found much smaller between the two thicker films, Behle *et al.* (1996). This is one of the sources of error pursued further in this paper.

2.2.7. *Temperature gradient in the TLC film*

Since the TLC film is partially transparent, it is obvious that a temperature gradient in the film will present to the observing camera a combination of the different colors exiting along the gradient direction. The consequently read temperature thus represents some type of average rather than a surface temperature. For example, for a steady heat flux of 20 kW/m^2, the temperature difference across a 20 μm thick TLC film with the heat conductivity of 0.2 W/(K m) is from Fourier's law 2°C, Ireland & Jones (2000). Gradients may also arise from transient temperature changes.

2.2.8. *Electric fields, pressure and acceleration*

No temperature measurement errors were found due to the presence of electric fields up to 150 kV/m, Evans *et al.* (1998). Pressures up to 133 bars were found to have no effect on encapsulated TLC's (quote from Ireland & Jones (2000)), neither had rotation/acceleration up to 1.6×10^4 g, Syson *et al.* (1996).

2.2.9. *The digital resolution*

The digitized R , G, and B values in combination with the unique color response for a TLC produce a digitized hue and a digitized read temperature. A common representation for digital images is 3×8 bits digitization of the R , G, and B. A test using a sheet of the TLC R25C5W (26 to 43°C) resulted in a hue resolution of 8 bits or higher, except in the dark blue region, where it decreased to about 6 bits, Behle *et al.* (1996). This in one of the sources of error pursued further in this paper.

Another digital error may arise from the spatial resolution of the image acquisition. The minimal number of pixels per unit length of the TLC surface depends on the magnitude of the temperature gradients: locations, with large gradients may require more pixels.

2.2.10. *Measurement noise*

Like any measurement, TLC temperature measurement has some noise. Temporal noise is reduced by averaging several images of the same area taken at

different times, and averaging over 10 images or more was found adequate, Farina & Hacker (1994), Behle *et al.* (1996). Local noise is reduced by averaging at several adjacent pixels, done by using a median filter, Baughn *et al.* (1999). An average over 5×5 pixels reduced the local noise from 3% to 0.9%, while a combination of time and spatial averaging reduced the noise from 3% to 0.6%, Behle *et al.* (1996).

2.2.11. *Accuracy of TLC measured temperatures*

A compilation of measured temperature errors using wide band TLC's, was presented in the review by, Smith *et al.* (2001), showing it to vary within the TLC temperature range, with a mean uncertainty within 2% to 9% of the effective TLC temperature range. The uncertainties can be estimated over an isothermal test surface with 95% confidence interval, as twice the standard deviation in the temperature. The lowest errors were reported for an in-situ and pixel by pixel calibration technique, using a series of images of isothermal surfaces, Sabatino *et al.* (2000).

Other calibration techniques have also been tested: a temperature-controlled mini calibrator for use in-situ, therefore, including the effects of the local light conditions and the view angle, Elkins *et al.* (2001) and in another technique, the optical system was calibrated instead, using a standard color chart, a mathematical algorithm and a reference TLC temperature - hue relation, Farina & Hacker (1994).

In another investigation it was indicated that the characteristics of the temperature - hue relations can be similar for different TLC's, and a dimensionless temperature, which collapse the temperature - hue relations from three different TLC's, (R29C4W, R40C5W, R40C15W), to a single curve was defined, Hay & Hollingsworth (1998).

3. The experimental setup

The calibrations of the thermochromic liquid crystals TLC's were performed where they were applied on a solid aluminum block (20×6×236 mm), which was placed inside a closed box, with a lid made of Plexiglas giving optical access from outside. The aluminum block was equipped with a flat electrical heater foil, which was glued to almost the full area of its lower surface, and a reference Pt-100 thermometer was mounted centered inside the aluminum block with thermal conductive grease.

One of the two larger aluminum surfaces was first spray-painted black, and the paint allowed to dry before the TLC application. A mixture of two volume parts of TLC mixed with one part of tap water was applied on the painted surface, using an airbrush with a nozzle diameter of 0.35 mm, with 1.8 bar feed air pressure.

A TLC film was created by spraying a number of thin layers, in a similar manner each, on top of each other, where each layer is allowed to dry before the next one is applied on top of it. This technique gives better control of film thickness magnitude and uniformity than one where a thick film is applied all at once.

The TLC material used was Hallcrest micro encapsulated chiral nematic of type BM/ R45C10/ C17-10 with a measured effective temperature range 47- 63°C, which is an interval in which hue is monotonically increasing with the temperature. Eight films of it were applied on the aluminum block side by side, each in a different thickness as shown in Table 3, which served to examine the effect of film thickness on performance and errors. The thickest film was made from 17 TLC layers, and the total measured thickness of this film was 38 μm. Each layer was thus approximately 2.2 μm thick (estimated average, the microcapsules may be somewhat larger).

TABLE 1. Number of sprayed TLC type R45C10 layers and the TLC film thickness, as used in the experiments.

Number of layers:	4	5	7	9	11	13	15	17
Thickness in μm:	9	11	16	20	25	29	34	38

A 3-CCD digital color video camera, SONY DCR- TRV 900E, was used in the experiments. Some critical camera settings were controlled by the user, by using manual settings; the white balance was set to the fixed value (indoor light), and the shutter time, and the aperture were set to fixed values. The "progressive scan" mode was activated, which allowed the camera to record images using all pixels at the same time.

The light source used was a Philips EXZ halogen lamp, 24°, 12 V, 50 W, with built in UV and IR filters, mounted 70 mm from the camera lens, parallel to the optical path between the lens and the TLC (Fig. 2). The distance between the camera lens and the TLC surface was 1080 mm. The angle ϕ between this nearly coaxial lighting-viewing arrangement, measured from the normal to the TLC surface, was 23°. Visual observation indicated that the light distribution over the TLC surface was uniform. A black cover was placed over the experimental system to prevent surrounding light sources and reflections from illuminating the target.

3.1. *The experimental procedure*

The temperature of the TLC-coated aluminum block was initially maintained at 55°C for 10 minutes, after which photos of the TLC were taken. The block was then again held at 55°C for about 45-50 minutes. The first of three full calibrations of the TLC was performed after this heating period. The start

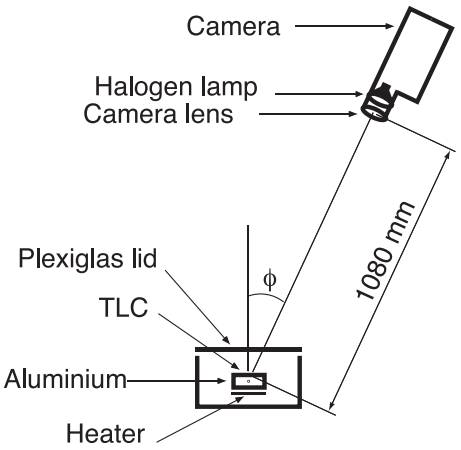

FIGURE 2. The experimental setup.

temperature for the calibration was well below the TLC red color start temperature, where the TLC is transparent (the black paint can be seen through the TLC). The TLC temperature was then raised in 16 steps within 10-15 minutes to the upper temperature limit, where the TLC turned from blue to transparent again. At each temperature level, a photograph of the TLC was taken, with the camera aperture set to F3.4.

The TLC was then kept at 55°C for 60- 65 minutes before the second calibration, which was performed in the same way as the first, but the camera aperture was now set to "open", because of some darkening of the TLC since the first calibration. The TLC was again kept at 55°C for 115-120 minutes before the third full calibration was performed. The color images captured during the calibrations were transferred using firewire (IEEE 1394) to a Macintosh computer, and the software Radius Photo DV. The images were then stored into bitmap files, having 510×680 pixels and 3×8 color resolution.

Hue H was calculated from the R , G, and B values of the recorded image , using Eqs. (1- 4). Hue obtained from this operation was for each TLC film averaged over a 28 mm^2 TLC area containing 1500 pixels, and was then fitted to the temperature using linear interpolation followed by a polynomial fit.

4. Experimental results

4.1. *Effect of light intensity on hue*

An important question is whether hue is dependent on the light quantity I into the camera CCDs. Hue H, which is calculated using Eqs. (1- 4) indicate that hue is not dependent on the light quantity for cases where R , G and B respond linearly to the light quantity.

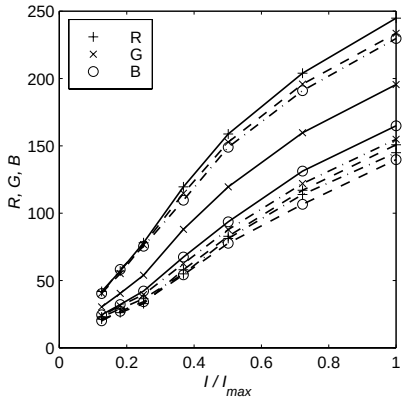

FIGURE 3. R, G and B values for different relative quantities of light I/I_{max} into the camera and for three different colored test surfaces, (-) the red surface, (- -) the green surface, (-.-) the blue surface.

The response was investigated for the camera, by varying the light and taking photos of three differently colored test surfaces, a red surface for which $R >$ (G, B), a green surface for which $G>$ (R , B) and a blue surface for which $B>$ (R , G). The colors of these surfaces were similar to those typically received from a 20 μm thick TLC film, using the present equipment. The light quantity was varied by changing the camera aperture number n, with all other camera settings kept fixed, I is proportional to $1/n^2$. The aperture number was varied from n= 9.6 to 3.4 at a constant shutter time of 1/75 s, hence varying the relative amount of light I/I_{max} from 0.12 to 1.0.

The measured color intensities R , G, and B (dimensionless in the range 0-255) were increasing with the light quantity as expected, and as can be seen in Fig. 3. The increase is non-linear, with its rate diminishing for the larger light levels. Hue at the highest light level I/I_{max}= 1.0 was calculated from these R , G and B values and found to be H= 0.064 , 0.314, and 0.647 for the red, green and blue surfaces, respectively.

The difference in hue at lower light levels from hue at the highest light level, are displayed in Fig. 4. It is seen that hue indeed varied with the light intensity, and in an irregular way for the different colored test surfaces. The maximal change in hue due to the 88% decrease in the light quantity was found to be 0.025, which is 4% of the useful hue range for the typical TLC films studied in this report. The result compares well with past studies, Behle *et al.* (1996).

In the upper range of the light levels for which; $120 < \max(R, G, B) < 255$, the maximal change in hue was only 1.5% of the hue range. All these changes are of the same order as those arising from the color digitization errors discussed

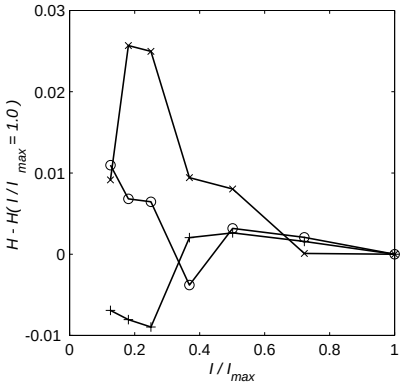

FIGURE 4. Variation in hue for different light quantities into the camera, measured on three different colored surfaces, (+) a red surface, (x) a green surface, (o) a blue surface.

below, and were possibly also in part caused by these. To minimize these two possible errors, the max(R ,G,B) level should therefore be maintained in the upper half of the R ,G,B range.

4.2. *The effects of the TLC film thickness*

Our measurements have confirmed past investigators' observations that the TLC film thickness cause changes in the TLC color response to the temperature, and this effect was therefore investigated in more detail. The R , G and B values in the images were measured as a function of the temperature, and are shown in Fig. 5 for the TLC R45C10 for the film thickness of 9 and 38 μm.

R was seen to be dominant in the lower temperature range, G in the temperature mid- range, and B in the higher temperature range. Noteworthy is the fact that the R , G, and B levels were higher for the thicker TLC film. The measured relation between T and H for the film thicknesses of 9, 11, 20, and 38 μm is shown in Fig. 6. It exhibits considerable and somewhat inconsistent variation with the TLC film thickness. For a fixed hue value in the upper part of the TLC temperature range, a thicker TLC film shows a higher temperature reading, but the opposite appeared in the lower part of the TLC temperature range. Between these two temperature intervals, there is a narrow region where hue was almost constant for all thicknesses.

The greatest sensitivity of the temperature to the TLC film thickness was found in the central green part of the TLC range, at about H= 0.37, and the indicated temperatures at this hue was investigated more closely, with results shown in Fig. 7. The indicated temperatures are seen to decrease with increasing TLC film thickness, and the highest rate of change was found for the thinner TLC layers. The indicated temperature difference between the TLC

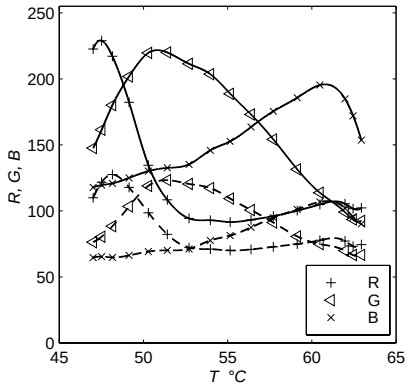

FIGURE 5. Measured R, G and B at different temperatures for TLC R45C10, after an aging period of 70 minutes at 55°C. The curves were fitted to the measured data. TLC film thickness, 9 μm (- -), 38 μm (-).

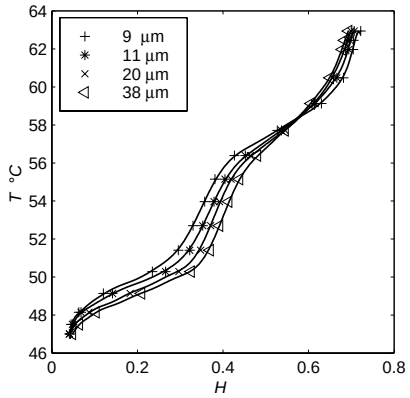

FIGURE 6. Hue as a function of temperature for different TLC (R45C10) film thicknesses (the curves were fitted to the measured data).

film thicknesses 9 and 20 μm, was found to be 12% of the TLC temperature range, and it was found to be only 7% between the thicknesses of 20 and 38 μm. The sensitivity in the indicated temperatures to variations in the TLC film thickness was therefore considerably lower for the thicker layers. These figures compares well with other experimental data, Behle *et al.* (1996).

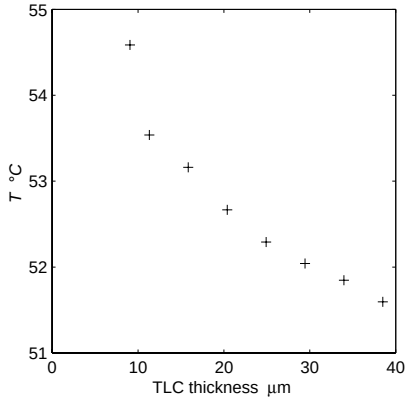

FIGURE 7. Evaluated temperatures for varying TLC thickness, at the value of h = 0.37 that gave the largest variation in temperature due to thickness change.

Since even the thickest film, 38 μm, would generate a temperature drop of only 0.1°C between the aluminum-film interface and the TLC film external surface, this heat conduction phenomenon can not account for the above-observed much higher hue-thickness dependence.

4.3. *The effect of TLC aging*

Our experiments indicated that the TLC temperature-color relationship change with time in normal use, and the aging of the TLC was therefore investigated in more detail. The stability of the complete system was investigated, including light, camera, reference thermometer and TLC, using the TLC C35R20 (36-64°C), which was sprayed on the aluminum block in a few layers until the TLC surface appeared rather grey, (i.e. obscuring the black primer color, probably about 30- 40 μm thick).

Four different full-range calibrations were then performed within six days, with the TLC stored in normal room conditions between these calibrations. The maximal difference in the temperatures indicated, for all hue values, was 0.4°C, which is 1.4% of the effective TLC temperature range. This provides an estimate of the stability of the whole measurement system, including any possible effects of the TLC aging at room temperature during the test period.

The temperature - hue relation as a function of time (aging) of the TLC was further investigated at more elevated temperatures. The TLC R45C10 was used in these tests in different thick films, (Table 3). During the test the TLC was held at 55°C, which is roughly in the middle of the temperature range of this TLC, and the temperature - hue relations were measured after 70 and 275 minutes of heating and are shown in Fig. 8. Aging is seen to be considerably

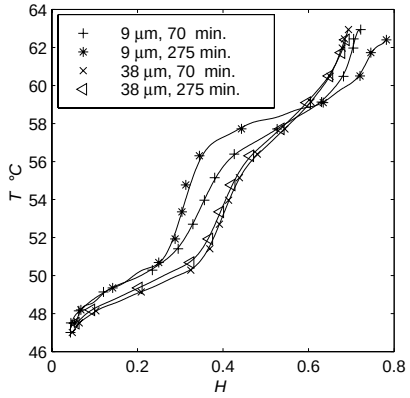

FIGURE 8. Temperature - hue relations for the TLC R45C10, measured after two different aging periods at 55°C, and for two different TLC layer thicknesses.

stronger for the thinner TLC film, and to have a qualitatively similar effect to that of the film thickness, on the temperature - hue relation shown earlier.

The aging was investigated more closely at $H = 0.37$, where it had the maximal effect on the temperature - hue relation. The temperature differences at this hue, in the period between 70 and 275 minutes of heating, were evaluated using the fitted temperature - hue data curves from our experiments, and are shown in Fig. 9. The aging effect was seen to diminish as the film thickness increased. The relationship is non-linear, accelerating significantly for the thinner films. For the thinnest film (9 μm), the temperature difference was found to be 2.2°C, and for the thickest one (38 μm) 0.50°C. That is 13% and 4%, respectively, of the effective TLC temperature range. Hence, the effects of aging can be reduced by applying thicker TLC coatings.

The change of the temperature hue relationship with time of the 20 μm thick TLC was investigated more closely. The temperatures were read from the curves fitted to the measured temperature - hue data at $H = 0.33$, measured at 10, 70, 145 and 275 minutes of heating at 55°C. The differences between these temperatures and the temperature read after 10 minutes of heating, are shown in Fig. 10. The temperature differences (i.e., the aging error) increased with time, while the rate of change decreased with time. Furthermore, the TLC was also becoming darker during this test period, measured as a 25% decrease in max(R,G,B), measured at a constant camera aperture setting.

4.3.1. *The digital resolution*

An interesting question is how disturbances in the light propagate into R , G and B values, and thereby further into hue and then into the read TLC

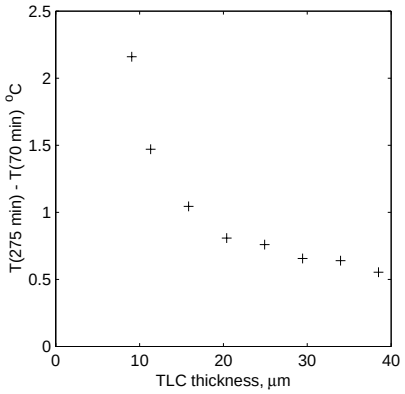

FIGURE 9. The read temperature differences between 275 and 70 minutes of heating at 55°C and for different TLC film thicknesses, at H= 0.37 for the TLC R45C10.

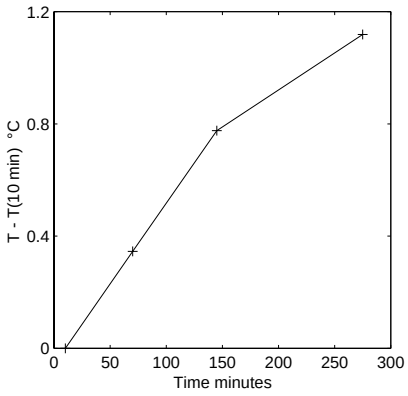

FIGURE 10. The differences between the read temperature at times between 10 and 300 minutes, and that read at 10 minutes from the start of heating period. In which the temperature was maintained at 55°C, for a 20 μm thick TLC R45C10 film, at H =0.33.

temperatures. Hue H is a function of R , G, and B, as expressed by Eqs. (1-4) and its derivatives indicating that the sensitivity in H to disturbances in R , G, and B will decrease with an increase in the difference, max(R,G,B)-min(R,G,B). It is therefore of interest to keep that difference as large as possible.

One disturbance comes from the digital image representation of R, G and B, which propagates into H and further into the TLC measured temperatures

T . Recall that the R,G,B values are obtained in 3×8 bits, as integers in the range 0- 255. Curves fitted to the measured R,G,B values as a function of the temperature, shown in Fig. 5, were expressed as integers in the range 0- 255, hence simulating the present digital image representation.

Hue was calculated from these integer values, and the steps in hue, ΔH, were found to be for the 9 μm thick TLC film within 0.008, for the 20 μm thick film within 0.004 and for the 38 μm thick TLC film within 0.003. Temperatures were then calculated from hue, using the fitted temperature - hue relations seen in Fig. 6.

The resulting temperature steps ΔT were found to vary within the TLC temperature range. Maximal values were identified within each temperature interval of 0.5°C and giving the trend shown in Fig 11. Three maxima were found, in the lowest red region, in the green region, and the largest values were found in the upper blue region. For the 20 μm and 38 μm thick TLC films, the maximal ΔT was about 1%, and the average about 0.5% of the effective TLC temperature range. These figures compare well with previous investigators experimental data, Behle *et al.* (1996).

The effect was larger for the thinner, 9 μm, film with maximal and average values of about 3% and 1%, respectively. Films thinner than 20 μm reflected less light and the difference max(R,G,B) - min(R,G,B), was therefore smaller, which may had increased the error. It is interesting to note that comparison of Figs. 6 and 11 shows a direct correlation between the derivatives dT/dH and the temperature measurement error ΔT; the error was larger for a locally larger derivative dT/dH . Consequently, it is expected that temperature measurement errors due to digitization can be made more uniform throughout the used temperature range for TLC-s that have a more linear temperature - hue relation. The value dT/dH may be used for a rule of thumb for limiting these errors.

Characterizing the non-linearity by the parameter $[dT/dH]/[dT/dH]_{av}$ it was observed in the present tests that its magnitude was within 3.0 for all the TLC films thicker than 20 μm. Ratios larger than this will further magnify the local errors. While the 3×8 bit digital representation of the R,G,B values is standard for color images, the error will be reduced if more bits are used. One more bit will halve the error and two more bits will halve it again.

5. Conclusions

TLC coating by spraying a number of thin layers on top o each other gives better control of film thickness magnitude and uniformity than one where a thick film is applied all at once.

The 3×8 bits digital image color representation produced a temperature measurement error of typically 1% of the effective TLC temperature range, for

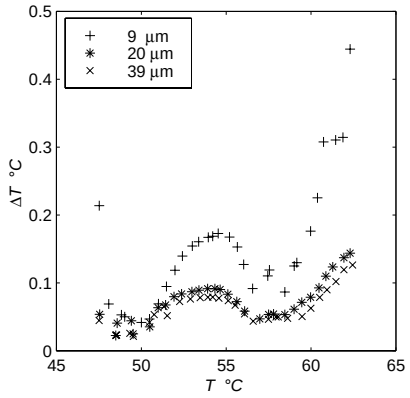

FIGURE 11. Changes in the indicated temperature as a result of a simulated 3×8 bit digital representation of the R, G, B colors, based on measured R, G, B- temperature relations for three different TLC film thicknesses.

films 20 μm or thicker, while the error was up to three times higher for thinner TLC films.

The digitization error increased with dT/dH , a more linear T - H relation may therefore make the error more uniform within the TLC temperature range.

An 8-fold variation of the light intensity into the camera produced variations in hue that were of the same order as the errors due to the digitization.

The indicated maximal temperature difference, at a constant hue, between a 9 μm and a 20 μm thick TLC film was found to be 12%, and between 20 and 38 μm 7%, of the effective TLC temperature range. The sensitivity to film thickness variation was thus lower for the thicker layers.

Maintenance of the TLC at 55°C (a temperature in the middle of the TLC reading range) for 205 minutes has shown, that at constant hue, the maximal read temperature change was for a 9 μm thick TLC film 13%, and for a 38 μm thick TLC film 4%, of the effective TLC temperature range. It can thus also be seen that the detrimental effects of aging are reduced for thicker TLC film.

Within the investigated range, thicker films are less susceptible to aging and thickness nonuniformities.

6. Acknowledgments

This work was partially supported by AGA AB (now Linde Gas), SKF Engineering and Research Center, B.V., the Volvo Research Foundation, and Volvo Personvagnar Komponenter AB.

References

Akino, N., Kunugi, T., Ichimiya, K., Mitsushiro, K. & M., U. 1989 Improved liquid-crystal thermometry excluding human color sensation. *J. of Heat Transfer* **111**, 558–565.

Baughn, J., Anderson, M., Mayhew, J. & Wolf, J. 1999 Hysteresis of thermochromic liquid crystal temperature measurement based on hue. *J. of Heat Transfer* **121**, 1067–1072.

Behle, M., Schulz, K., Leiner, W. & Fiebig, M. 1996 Color-based image processing to measure local temperature distributions by wide-band liquid crystal thermography. *Appl. Sci. Research* **56**, 113–143.

Birrell, D. C. & Eaton, J. K. 1998 Liquid crystal temperature measurement for real-time control. In *SPIE Conf. Applications of Digital Image Processing XXI, San Diego California*, , vol. 3460, pp. 58–66.

Camci, C., Kim, K. & Hippensteele, S. A. 1992 A new hue capturing technique for the quantitative interpretation of liquid-crystal images used in convection heat transfer studies. *J. Turbomach.* **114**, 765–775.

Chan, T., Ashforth-Frost, S. & Jambunathan, K. 2001 Calibrating for viewing angle effect during heat transfer measurements on a curved surface. *Int. J. of Heat and Mass Transfer* **44**, 2209–2223.

Elkins, C. J., Fessler, J. & Eaton, J. K. 2001 A novel mini calibrator for thermochromic liquid crystals. *J. of Heat Transfer* **123**, 604–607.

Evans, M. K., Rapley, C. W., Wilcock, D. W. & Sheldrake, T. H. 1998 A study of microencapsulated chiral nematics in the presence of electric fields. *Int. J. of Heat and Mass Transfer* **41**, 3685–3687.

Farina, D. J. & Hacker, J. 1994 Illuminant invariant calibration of thermochromic liquid crystals. *Exp. Thermal and Fluid Science* **9**, 1–12.

Fergason, J. L. 1968 Liquid crystals in nondestructive testing. *Appl. Optics* **7**, 1729–1737.

Hay, J. & Hollingsworth, D. 1996 A comparison of trichromic systems for use in the calibration of polymer-dispersed thermochromic liquid crystals. *Exp. Thermal and Fluid Science* **12**, 1–12.

Hay, J. L. & Hollingsworth, D. K. 1998 Calibration of micro-encapsulated liquid

crystals using hue angle and a dimensionless temperature. *Exp. Thermal and Fluid Science* **18**, 251–257.

Herold, W. & Wiegel, D. 1980 *Problems of the Photographic Documentation of Liquid Crystalline Thermographs*, pp. 1255–1259. Pergamon Press, Oxford.

Ireland, P. & Jones, T. 2000 Liquid crystal measurements of heat transfer and surface shear stress. *Meas. Sci. Technol.* **11**, 969–986.

Ireland, P. T. & Jones, T. V. 1987 The response time of a surface thermometer employing encapsulated thermochromic liquid crystals. *J. Phys. E: Sci. Instrum.* **20**, 1195–1199.

Sabatino, D., Praisner, T. & Smith, C. R. 2000 A high-accuracy calibration technique for thermochromic liquid crystal temperature measurements. *Experiments in Fluids* **28**, 497–505.

Smith, C. R., Sabatino, D. R. & Praisner, T. J. 2001 Temperature sensing with thermochromic liquid crystals. *Experiments in Fluids* **30**, 190–201.

Syson, B. J., Pilbrow, R. G. & Owen, J. M. 1996 Effect of rotation on temperature response of thermochromic liquid crystal. *Int. J. Heat and Fluid Flow* **17**, 491–499.

Wiberg, R., Muhammad-Klingmann, B., Ferrari, J. & Lior, N. 2000 Use of thermochromic coatings for the experimental determination of the distribution of heat transfer coefficients in gas-cooled quenching. In *Proc. 5th ASM Heat Transfer and Surface Eng. Conf. in Europe., Gothenburg, Sweden*, pp. 275–286.

Paper 2

P2

Heat transfer from a cylinder in axial turbulent flows

By Roland Wiberg[*] and Noam Lior[**]

[*]FaxénLaboratoriet, Dept. of Mechanics, KTH, SE-100 44 Stockholm, Sweden
Email: roland@mech.kth.se
[**]Dept. of Mechanical Engineering and Applied Mechanics, University of Pennsylvania, Philadelphia, PA 19104-6315, U.S.A.

To be submitted

Local convective heat transfer coefficients were measured on a two-diameter long cylinder in axial flows of air, at Reynolds numbers of $8.9\times10^4 < Re < 6.17\times10^5$ (9 to 63 ms$^-$1), using thermochromic liquid crystals (TLC) and a electrically heated foil consisting of thin metal bands. The flow in front of the cylinder was modified by the use of a turbulence generating grid, and by inserts, circular discs of two sizes, in front of the cylinder. These create a major change in the local convective heat transfer coefficient distribution on the cylinder. Increase of the turbulence intensity from $Tu < 0.1\%$ to 6.7 % at the same Re, increased the average calculated Nusselt number Nu over the cylinder by 25%, and decreased the Nu non-uniformity (σ_{Nu} and σ_{max}) by 30% and 12% respectively. One of the flow modification inserts reduced σ_{Nu} by 25%. The position of flow reattachment was measured using tufts, and the envelope of the flow separation region was successfully visualized by a specially TLC-based heated flat plate mounted in the flow above the cylinder. Correlation's between the Nu and Re in the form $Nu = CRe^e$ were established and presented for the average Nu on the three different cylinder surfaces, and the variation of the local exponent e was shown along the cylinder.

Key words: flow across bluff bodies, circular cylinder in axial flow, convective heat transfer, thermochromic liquid crystals, flow visualization

1. Nomenclature

a, b, c, d, e, f: positions on the cylinder.
D: outer diameter of the cylinder.
h: local convective heat transfer coeff., $\mathrm{Wm^{-2}K^{-1}}$.
$\overline{h}$: surface averaged convective heat transfer coeff.
k_∞: heat conductivity of the upstream air, $\mathrm{Wm^{-1}K^{-1}}$.
L: length of the cylinder.
Nu: local Nusselt number, dimensionless.
$\overline{Nu}$: surface average of Nu, dimensionless.
Nu_{max}, Nu_{min}, extremes values of Nu along a-d.
R: outer radius of the cylinder.
r: radius.
Re: Reynolds number, dimensionless.
T: local surface temperature.
T_∞: upstream air temperature.
TLC: Thermochromic Liquid Crystals.
Tu: free stream turbulence, dimensionless.
U_∞: upstream time-averaged air velocity (in x direction), $\mathrm{ms^{-1}}$.
u': the fluctuating component of the upstream (free stream) air velocity (x-direction), $\mathrm{ms^{-1}}$.
q'': electrically supplied surface heat flux, $\mathrm{Wm^{-2}}$.
x, y: coordinates.

1.1. *Greek symbols*

ν_∞: kinematic viscosity of the upstream air, $\mathrm{m^2s^{-1}}$.
σ_{Nu}: surface weighted relative standard deviation in Nu [Eq. 6], dimensionless.
σ_{max}: relative max - min difference in Nu, dimensionless.

2. Introduction

It is of interest to know convection heat transfer coefficient (or Nusselt number) distributions over surfaces of blunt bodies in high speed flow in many diverse applications, including cooling of electronic equipment, cooling or heating of foodstuffs, and gas-cooled quenching. The latter is a topic of extensive study at the FaxénLaboratoriet of the Royal Institute of Technology, Sweden (Lind *et al.* (1998) Thuvander *et al.* (1999) Wiberg *et al.* (2000) Wiberg & Lior (2003) Ferrari *et al.* (2003) Vynnycky *et al.* (2003) Lior (2003)).

In quenching, the product hardness, uniformity of mechanical properties, and shape distortion depend on the rate and uniformity of the cooling. Gas quenching requires high gas speeds and pressures (typical values are at least 10 ms^{-1} and 10 bar, but they vary widely depending on the application), i.e. turbulent flows with Reynolds numbers typically between a few hundred thousand to a few million. The flows are thus highly turbulent, with separations and reattachments, which create significant convection heat transfer coefficient non-uniformity over the body surface. These coefficients must be controlled in magnitude and uniformity to obtain optimal quench products.

In this paper we report on measurements of the temperature and Nusselt number distributions over the surfaces of a cylinder with a length to diameter ratio $LD^{-1} = 2.00$ at Reynolds numbers in the range, $8.9{\times}10^4 < Re < 6.17{\times}10^5$, in axial flows where the approaching free stream is not modified by any upstream turbulence generators or other objects, and in axial flows affected by a turbulence generating grid, and in some cases by flow modification inserts (circular discs) upstream of the cylinder. Information about the nature of the flow along the cylinder is also provided.

While there exists a fair number of experimental studies that provide Nu distributions for single cylinders (cf. Lowery & Vachon (1975) , Achenbach (1975) for $3{\times}10^4 < Re < 4{\times}10^6$, Zukauskas & Ziugzda (1985), Zdravkovic (1997), Zdravkovic (2003)) and multiple ones (cf. Achenbach (1989)) in cross flows, little information is available for cylinders in axial flow, and none were measured for $Re > 5.5{\times}10^4$.

In experiments with axial flow along a cylinder, Sparrow & Geiger (1985) measured the mass transfer Sherwood numbers over the cylinder upstream (front) surface by using the naphthalene sublimation technique, for $5{\times}10^3 < Re < 5 \times 10^4$ and at Tu= 0.5%. Employing the mass heat transfer analogy, (the relation between the Sherwood number Sh, Nusselt number Nu, Prandtl number Pr and the Schmidt number Sc) to correlate the average Nu over this surface as

$$\overline{Nu} = 1.05 Pr^{0.36} Re^{1/2} \tag{1}$$

The local convection mass/ heat transfer from the surface, was found to increase from the center of the surface towards the outer radius, and was found at the edge to be 2.2 times higher than at the center and independent of Re, which indicated that Nu increased as $Re^{0.5}$ over the entire surface.

Measurements of Nu on the round surface of the cylinder, at constant surface heat flux, in axial flow, were performed for $2.52{\times}10^4 < Re < 5.36{\times}10^4$, Tu= 0.8% and LD^{-1}= 13, by Ota and Kon (1977), and for $8{\times}10^3 < Re < 4.7{\times}10^4$, Tu= 0.5% and LD^{-1}= 10, by Sparrow et al. (1987). In these studies, Nu was found to have a maximum at the distance 3 R downstream from the

front edge, then decreasing monotonically along the axis. For Re lower than 3.0×10^4 the maximum were found to occur somewhat closer to the front edge.

Velocity and turbulence measurements of the flow around a circular cylinder in an axial flow were performed by Kiya *et al.* (1991) for $Re= 2 \times 10^5$, Tu <0.2, $LD^{-1}= 10$, and by Ota (1975)), who also measured Nu, for 4.08×10^4 < Re < 6.8×10^4, Tu =0.8 %, $LD^{-1}= 10$. These investigations showed that the flow separated at the front edge and reattached to the surface at or slightly downstream of the maximum in Nu.

Our paper also investigates the effects of circular discs inserted upstream of and parallel to the cylinder front on the flow and heat transfer over the cylinder in axial flow. No such studies were found in the literature, although an extensive investigation was performed on their influence on the drag coefficient, Koenig & Roshko (1985), for $1\times10^5 < Re < 8\times10^5$, which included flow visualization. They found that an optimal choice of disc diameter ($0.75D$) and distance ($0.375D$) from the cylinder front, reduced the total drag coefficient for the cylinder front and disc together from 0.72 to 0.01, which is comparable to that for a body without flow separation. The results were found to be independent of the Reynolds number and the disc surface roughness. The same drag reduction was also found for a rough cylinder front surface, preventing laminar separation, when the front edge had a radius of $1/4$ R.

3. The experimental method

The "Minimum Turbulence Level" closed loop wind tunnel at the Department of Mechanics at KTH (cf. Lindgren & Johansson (2002)), was used for the measurements. The turbulence level at the test section inlet is Tu <0.1%. It has a 7-meters long and a 800×1200 mm wide test section (which in this study had a constant flow cross section from the inlet and over the test cylinder), and a Plexiglas window for visual access from outside, see Fig. 1.

An opening slit in the roof of the test section (downstream of the cylinder) maintained the pressure atmospheric. During all the measurements, the upstream flow velocities were in the range 9 to 64 ms^{-1}, and at temperatures of 25 to 28 $^\circ C$, while the cylinder surface temperatures were within the active range of the thermochromic liquid crystals, 36 to 63 $^\circ C$, used for the surface temperature measurement and flow visualization. The blockage based on cross section area of the cylinder in the test section was 2 %.

The measurement of the convection heat transfer coefficient distribution on the cylinder surfaces was made based on eq. 2. A constant and known heat flux q'' was generated electrically in a thin foil applied to the cylinder surface, and the surface temperature distribution on the foil, T, was measured using thermochromic liquid crystals (TLC) coated on the foil.

$$h = \frac{q'' - 5.67 \times 10^{-8}(T^4 - T_\infty^4)}{T - T_\infty} \tag{2}$$

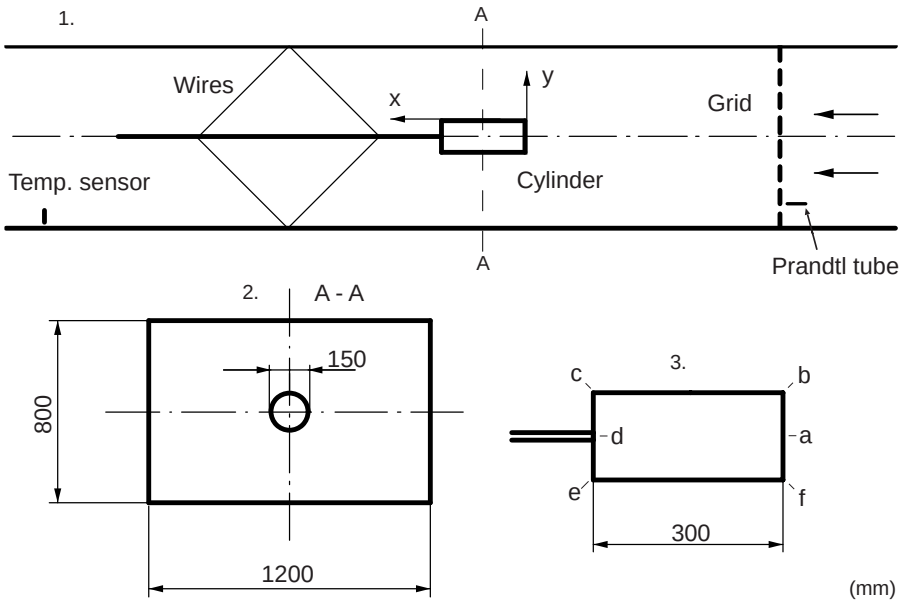

FIGURE 1. The wind tunnel experimental setup. 1. the test section with the cylinder inside. 2. cross section of the test section. 3. the cylinder; points a, b, c, d, e, f serve to identify locations along it.

These crystals change their color with temperature, and digital video photographs of the TLC were translated to temperatures by image processing software developed by us for this purpose, associated with a careful calibration.

A Sony DCR-TRV 900E camera, 680×510 pixels, 24 bit color resolution and two 24^o, 50 W halogen lamps fixed to the camera, were used for the photographs. The local surface temperatures T were evaluated from the colors and the convection heat transfer coefficient h was calculated using equation eq. 2, where the electrically supplied heat flux q'', was reduced by a calculated radiation loss, (in average over the cylinder typically 4 -10 % of q'', the lower values Re levels) and where T_∞ was the upstream air temperature. This estimation of the radiation from the cylinder is justified by the facts that the test section walls and the cylinder were painted black, and that the cylinder is small, 2 % of the cross section and 4 % of the length, compared with the test section.

3.1. *The test cylinder.*

The test cylinder (Fig. 1) had a diameter of D= 150 mm and length of L= 300 mm, it was made of solid extruded polystyrene (EPS), (k= 0.033 $\mathrm{Wm^{-1}K^{-1}}$) and machined by lathe to attain its cylindrical shape and to get the front

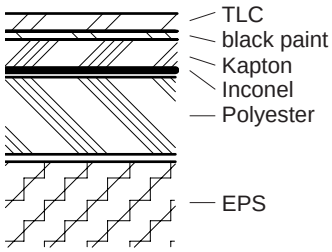

FIGURE 2. The cylinder surface with the TLC, backing paint, electric resistance foil, and thermal insulation.

surface perpendicular to the cylinder axis. Three thermocouples were mounted just under the EPS surface along b-c at xD^{-1}= 0.087, 1.00 and 1.913, and along a-b, at the radius rR^{-1}= 0.60. These were mounted using thin foils of aluminum 8 mm wide and epoxy glue to increase the thermal contact with the surface.

To make the cylinder surface smooth, a polyester film 125 μm (k= 0.033 $\mathrm{Wm^{-1}K^{-1}}$) was glued on the EPS surface, see Fig. 2, on top which an electrically conductive Inconel foil designed by us, (manufactured by Calesco Foil AB [1]), was glued over all of the cylinder surface, except for a distance within $0.01D$ (1.5 mm) from the cylinder edges and the cylinder support in the rear.

The foil consisted of many 1.5 mm wide flat bands of Inconel 12 μm thick, (k= 12 $\mathrm{Wm^{-1}K^{-1}}$, relative resistance 1.25×10^{-4} $\mathrm{K^{-1}}$), spaced 0.2 mm apart and embedded in one of the faces of a 50 μm thick polyimid film (k= 0.12 $\mathrm{Wm^{-1}K^{-1}}$). The uniformity in the resistance over the surface was tested by electrically dividing it into 42 parts, for which the resistance was found to differ by only $\pm$ 1.5 % from the average.

Black paint was sprayed on the foil, and then the micro encapsulated TLC of Hallcrest[2] type R35C20 C17-10 was sprayed on top of the paint in a 40 mm wide film, estimated 20 μm thick, along the cylinder f-a-b-c-d. Manually variable transformers (a.c.) were used to provide the foil with constant electric power, which was measured and found to vary within $\pm$ 1.5 % from the average during the experiments.

With the objective to measure the convection heat transfer coefficients on the cylinder surface, it was important to examine measurement errors due to axial conduction inside the cylinder core and surface layers, and ensure that they are within acceptable limits. A one-dimensional calculation along the surface was performed to estimate the heat flux in the EPS and all the foils, using the thickness and the thermal conductivity's of the foils and the measured surface temperature field.

[1]Calesco Foil AB Västeråsvägen 9 S-73040 Kolbäck Sweden
[2]Hallcrest 20 Downing Road, West Meadows Industrial Estate, Derby, UK, DE21 6HA.

Based on measured conditions in steady state, the effective thickness of the EPS cylinder core, through which axial conduction took place, was estimated to be 14 mm. The axial heat flux loss along the surface was then calculated to be over most of the cylinder within only 2 % of the electrically supplied surface heat flux used in Eq. 2 for determining h. Larger losses may exist within a distance of 0.15 R from the edges. The foil gave no heat within a distance of 0.04 R from the edges and the data were here therefore cancelled.

To assist the detection of flow direction, 8 mm long thin soft cotton tufts were taped on the surface in a row along the cylinder, 10 mm apart, each mounted perpendicular to the cylinder axis, and the visual observations were performed at $Re = 1.75 \times 10^5$.

A steel pipe $0.113D$ (17 mm) in diameter was glued into the cylinder end, at the center, for support in the wind tunnel , and the pipe was held by eight 2.0 mm thick steel wires, which centered and aligned the cylinder to be parallel to the test section walls. Despite the rigid support, it was estimated that the cylinder vibrated with a displacement of about ± 0.5 mm.

3.2. *The measured flow configurations.*

The measurements were performed in four different configurations: A) the cylinder alone in a low upstream turbulence flow, $Tu < 0.1$ % B) the cylinder in an upstream flow affected by turbulence-generating grid, $Tu = 6.7$ %, C) the cylinder placed downstream of a circular disc $1/3D$ in diameter, which was centered on the cylinder axis and located at $xD^{-1} =$ -1.00, D) the cylinder placed downstream of a circular disc $2/3D$ in diameter, at the same position.

The turbulence-generating grid was made of square rods 10 × 10 mm, 50 mm apart, and was located upstream of the cylinder at $xD^{-1} = -5.50$ ($x = -825$ mm). Configurations C) and D) were included to examine the effects of upstream bodies on the convection heat transfer coefficients and flow on the cylinder, which also at least partially addresses the conditions when a body to be quenched is part of a multi-body quench-charge. The upstream discs in these configurations were $0.0333D$ (5 mm) thick with sharp corners and fixed using 0.5 mm thick wires (in configuration (C): 5 or 6 wires, in configuration (D): 8 wires) to the test section walls. The position of these wires was chosen so that their possible wakes would not directly affect the areas on the measured cylinder. Special attention was given during the measurements to have the cylinder centered and parallel to the test section walls, and to have the discs parallel to the cylinder front surface.

3.3. *Calibration of the TLC.*

The TLC was calibrated before and after the measurements, in-situ on the cylinder and inside the test section, using the thermocouples in the cylinder surface as reference. Color photographs of the TLC were taken through the

glass window from a fixed position outside the test section, and special attention was taken to shield any light reflections and optical disturbances. The surface temperature was raised a few °C between each photography session, and the digital pictures were transferred from the camera to a Macintosh computer using fire wire (IEEE- 1394). The image was then further loaded using QuickTime (a Macintosh software) into Matlab5.2.1^{TM} [3], using its function *getvidframe*.

The color variable hue was calculated and related to the thermocouple measured temperatures. Possible local non-uniformity in the TLC color response along the cylinder was investigated, using an isothermal chamber, built for this purpose (having insulated walls of EPS a fan and a heater). Corrections were then applied to the in-situ measured temperature - hue relation for TLC areas in between the positions of the thermocouples. The position of the camera relative to the cylinder caused a varying pixel density in the image of the cylinder surface, which was corrected in the software. Many parameters affects a TLC temperature measurement, for further details concerning the TLC technique, see Wiberg & Lior (2003). All together, the errors in the local TLC measured surface temperatures were estimated to be within ± 1.2°C, compared to the true surface temperatures.

3.4. *The experimental procedure*

The wind tunnel was started, the upstream flow velocity U_∞ (measured using the Prandtl tube), and the flow temperature T_∞, were allowed to stabilize, the velocity within ± 0.5%, the temperature within ± 0.1°C. The electrical power generating the surface heat flux q'' of the foil was increased until the surface temperatures came within the active temperature interval of the TLC. The temperatures were then allowed to stabilize within ± 0.3°C as indicated by the thermocouples, typically over 10 minutes.

In the steady state, color photographs of the TLC were taken, using the same camera, view angle and light settings as were used during the in-situ calibrations, and the electrical current to the foil was then shut off. This procedure was repeated for each measurement.

The thermocouples were read and viewed by the use of a computer, which also could shut off the electric power to the foil, in case the temperature exceeded a fixed level, chosen near the upper limit of the TLC.

3.5. *Turbulence measurements*

The turbulence level (Tu) was measured using a hot wire anemometer with a single hot wire 2.5 μm in diameter, at the average flow velocity 18 ms^{-1}. At each position, data were evaluated from 4.8×10^5 samples taken during two minutes. Tu were for each of the investigated five x-position averaged from

[3]The MathWorks, 3 Apple Hill Drive, Natick, MA 01760-2098

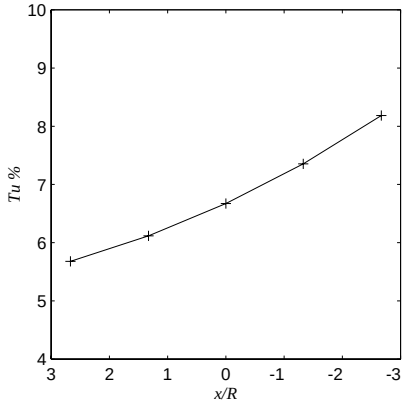

FIGURE 3. Measured turbulence intensity downstream of the turbulence generating grid used in configuration (B), without any cylinder in the test section, U_∞= 18 ms^{-1}.

measurements at four positions in the y, z plane. The turbulence level is defined, in Eq. 3, where U_∞ is the average velocity in the x- direction and u' the velocity fluctuations around the average in the same direction.

Tu measured in configuration (B), without any cylinder in the test section, can be seen in Fig. 3. Tu was found to decay downstream from the grid, and was at x= 0.00 m found to be Tu= 6.7%.

$$Tu = \frac{\sqrt{\overline{u'^2}}}{U_\infty} \tag{3}$$

3.6. *Data analysis*

The color photographs were evaluated from a $0.05D$ wide band of the TLC along the cylinder f-a-b-c-d, giving an array of hue values 1050 elements long, (f-a 150 elements, a-b 150 elements, b-c 600 elements, c-d 150 elements). Temperatures were then evaluated from the hue values, and then smoothed by averaging over each ± 8 adjacent elements (± 0.0267 D).

Based on these measured temperatures the coefficient h was calculated using Eq. 2, and further expressed in terms of a Nusselt number Nu (dimensionless), as can be seen in Eq. 4,

$$Nu = \frac{hD}{k_\infty} \tag{4}$$

where k_∞ is the heat conductivity of the upstream air. Area-weighted surface averages of Nu were calculated, along the front end surface a-b , along the middle surface b-c, along the rear end surface c-d and along the whole surface

a-b-c-d, ($\overline{Nu}_{a-d}$), where the values near the edges were omitted as explained above. The averages were evaluated assuming that Nu was symmetrical around the cylinder axis, using Eq. 5,

$$\overline{Nu} = \frac{\sum Nu_i A_i}{\sum A_i} \tag{5}$$

where A_i is a finite small area where the value is Nu_i, summarized along the surface of interest; a-b, b-c, c-d or a-d.

A non-uniformity number for the variation in Nu along the cylinder a-b-c-d, was calculated by means of the surface weighted relative standard deviation σ_{Nu}, seen in Eq. 6.

$$\sigma_{Nu} = \frac{[\frac{\sum (Nu_i - \overline{Nu}_{a-d})^2 A_i}{\sum A_i}]^{\frac{1}{2}}}{\overline{Nu}_{a-d}} \tag{6}$$

Another non-uniformity number based on max and min values of Nu along a-b-c-d was calculated as can be seen in Eq. 7, where Nu_{max} and Nu_{min} are the largest and smallest values of Nu along the surface a-b-c-d , respectively.

$$\sigma_{max} = \frac{Nu_{max} - Nu_{min}}{\overline{Nu}_{a-d}} \tag{7}$$

The Nusselt number was correlated with the Reynolds number Re, raised to the exponent e, where

$$Re = \frac{U_\infty D}{\nu_\infty} \tag{8}$$

and where ν_∞ is the kinematic viscosity of the upstream air, i.e.,

$$Nu = CRe^e \tag{9}$$

where C and e were unknown constants to be determined from the measurements. Nu was measured at three different Re, and C and e were calculated by finding the value of e which minimized the relative differences in C for these three Re.

It is noteworthy that a more complete correlation for Nu would also include the Prandtl number and for the flow stagnation region even the turbulence intensity level (cf. Zukauskas (1989) ch. 11). Since air was used in this study (constant Prandtl number), and the turbulence intensity was only one of 2 values, these dependences weren't included in Eq. 9.

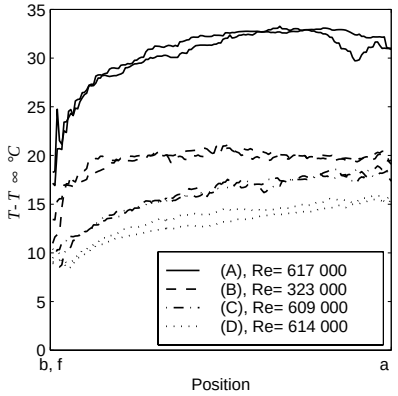

FIGURE 4. Examination of symmetry in the measured temperatures on the front (upstream) cylinder surface for the cylinder in different configurations (A), (B), (C), (D): in each pair of temperature profiles for the same Re, one is along line a-b and the other along a-f. (Before data smoothing).

3.7. *Error estimates*

The temperature measurements were performed on the cylinder in the configurations (A), (B), (C) and (D), at the highest Reynolds numbers for each of the configurations. For each case, two curves of non-smoothed data for the upstream (front) surface, from the center and towards the edge, along a-b and along a-f, are shown in Fig. 4. Since each pair of such curves is nearly identical, within the error range for the measurements, symmetry of the measurements is confirmed.

Based on error analysis, the error in the local Nu was estimated to be $\pm$ 7 %, in which the main source off error is in the TLC measured surface temperatures.

The static pressure difference between the flow upstream of the grid and in the room outside the test section, was measured to be <1% of the measured atmospheric room pressure. The velocity downstream of the grid may therefore, estimated differ from the velocity upstream of the grid by <1%. The displacement due to the growing test section wall boundary layers, may have increased the velocity over the cylinder in all configurations, estimated to be <1%. The final error in the Reynolds number was estimated to be $Re \pm 2\%$.

The error in e is such that Nu can be calculated within the error range above, for a value of Re, which is within the range for the measurements, using the found local constant e, a measured distribution of Nu and Eq. 10.

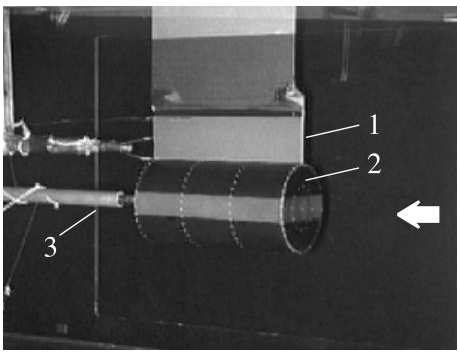

FIGURE 5. The cylinder inside the test section, with the flow visualization plate mounted above its surface, 1: the plate, 2: the cylinder, 3: the cylinder support.

$$Nu_2 = Nu_1(\frac{Re_2}{Re_1})^e \tag{10}$$

where Nu_1 is a measured distribution at Re_1 and Nu_2 the interpolated values valid at Re_2.

3.8. *TLC-based visualization of the flow along the cylinder*

To try to visualize the flow along the cylinder, a 300 mm long and 2.5 mm thick smooth Plexiglas plate was constructed to allow TLC temperature measurements over one of its faces. The plate was aligned with the cylinder axis and perpendicular to the cylinder surface, see Fig. 5. The front (upstream) plate edge was rounded and its lower edge was held ca 1 mm above the cylinder surface. An electrically heated foil, 300×83 mm (Inconel on Kapton, of the same type as used on the cylinder) was glued, with the Inconel side of the foil, to one of Plexiglas plate faces.

The foil was spray-coated with black paint and with a film of the TLC R35C20. A thermocouple was also glued on the foil, and used for in-situ calibrations of the TLC, before and after the measurements. The maximal change due to aging between the two calibrations, was found to be 0.9 $^\circ C$. The TLC surface was further tested in an isothermal chamber and non-uniformity over the surface were then found within $\pm$ 0.6 $^\circ C$.

During the measurements the power was increased to the foil until the surface temperature of the plate came within the active interval of the TLC, and was then held fixed to achieve a thermal steady state, which was indicated by the thermocouple reading. Color photographs of the TLC was captured, from which the surface temperature field was evaluated. The temperature data was smoothed over the plate, using a median filter over a square in size

0.1×0.1 R (cylinder radius), that was 14×14 image pixels. Data closer than 0.05 R from the plate edges are therefore less reliable.

Measurements were performed on the plate: in configuration (A) at Re= 1.75×10^5 and with the plate front edge at xR^{-1}= -0.50, 0.00, 0.13, 0.50, 1.00, 1.50, 2.00. In configuration (B) and (C), with the plate front edge at xR^{-1}= 0.00. During the measurements on the flat plate the cylinder was not heated, and no plate was inserted into the flow during any thermal measurements on the cylinder.

High convection heat transfer coefficients are then expected where the temperatures are low, and low convection heat transfer coefficients are expected at where the temperatures are high. The lowest temperature appearing on the surface was identified for each x- position along the plate, creating a unique curve on the surface of maximum convection heat transfer for each measurement.

4. Experimental results

4.1. *Measurements in configuration (A).*

Surface temperatures are visualized on the cylinder in configuration (A), and with the whole surface coated with thermochromic liquid crystals (TLC) and for U_∞= 63 ms^{-1}, $Re = 6.0\times10^5$ and $Tu < 0.1$ %. The surface temperatures $T - T_\infty$, can be seen in Fig. 6 in where the highest temperatures (lowest h) is seen on the upstream surface, while the lowest temperatures were found in the rear part of the cylinder along the surface b-c. The temperatures on the downstream end of the cylinder c-d, were found somewhat lower than these on the upstream surface. (Another TLC film was used for further measurements of Nu, as was described in the section about the test cylinder).

Measurements of the local Nusselt number (Nu) on the cylinder were performed at the low upstream turbulence levels ($Tu < 0.1$ %), and at Reynolds numbers (Re) of 6.17×10^5 , 3.22×10^5 and 1.77×10^5. Nu along the cylinder surface is shown in Fig. 7 and is seen to increase with Re, as expected, and the characteristic shape of the curves is similar for all Re. The average along the surface a-b-c-d , was for these three Re found to be, $\overline{Nu}_{a-d}$= 990, 640 and 430, respectively.

The average Nu is significantly higher along the surface b-c than on a-b, increasing from the front edge by at least two-fold to a maximal value at xR^{-1}= 3.0. On the downstream (rear) surface c-d, Nu drops to about half the previous values, increasing from the edge to the surface center. The latter behavior can be explained by the thermal consequences of wake formation on the downstream (rear) surface.

Using the tufts, it was found that flow reattachment along the cylinder surface b-c took place between xR^{-1}= 2.93 and 3.07, at Re= 1.75×10^5. This

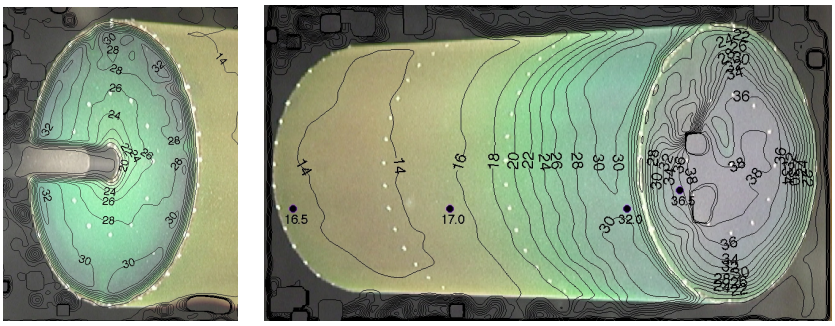

FIGURE 6. TLC measured temperatures ($T-T_\infty$) on the cylinder in configuration (A) and in an axial flow at $Tu < 0.1$ % and $Re = 6.00 \times 10^5$ ($U_\infty = 63$ ms^{-1}). Round dots: thermocouple-measured temperatures below the foil. (Some optical disturbances can also be seen on the upstream end, to the right in the figure).

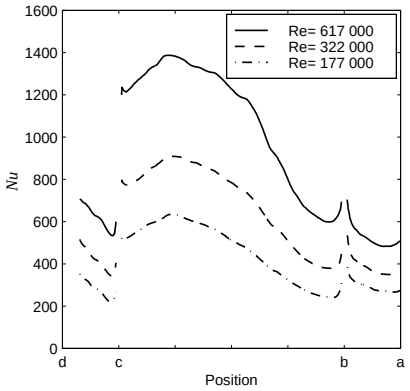

FIGURE 7. The Nusselt numbers along the cylinder surfaces, configuration (A), for different Re.

coincides with the position measured for the maximal Nu along the same surface, and is only somewhat shorter than the reattachment length, found by Kiya *et al.* (1991), who measured that position in terms of reverse flow intermittence (reverse-flow time = 0.5), which appeared at $xR^{-1} = 3.18$- 3.22. For Re and Tu similar to what was used here, while the cylinder was longer, LD^{-1}=10. Indicating that the cylinder used here was long enough to make the flow, in the separated region, independent on the cylinder length.

The temperature field on the heated and TLC-coated plate mounted above the cylinder surface b-c, with the plate upstream edge at $xR^{-1} = 0.0$, are shown

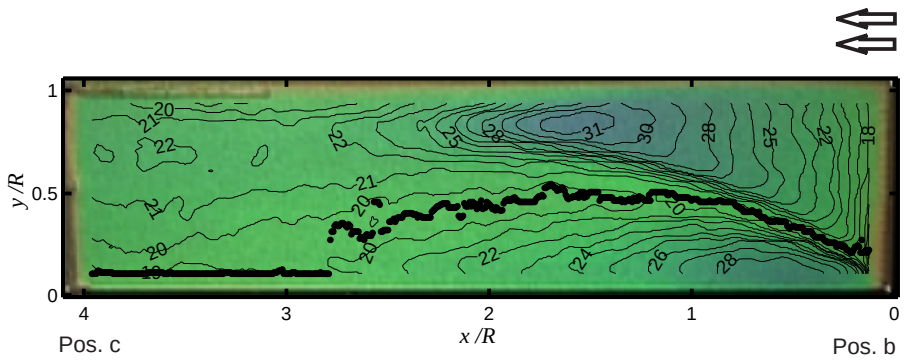

FIGURE 8. Isotherms ($T - T_\infty$), on the flow visualization plate mounted above the cylinder in configuration (A), Re= 1.75×10^5, $Tu < 0.1\%$. The minimal temperature locations are marked by the bold black dots.

in Fig. 8. The heavy curve in the figure shows the location of the minimal temperatures on the plates, which, as discussed above, coincides with the maximal convection heat transfer coefficient (h). It starts at the leading edge of the cylinder (position b), follows a curved path through a maximal height of y/R= 0.5 and descending to reach the cylinder surface at about xR^{-1}= 3, which is in the above mentioned flow reattachment region to the cylinder.

Velocities measured above a longer cylinder in an axial flow of Re= 5.62×10^4, Ota (1975), showed that the mean stream line (the dividing stream line), between the front edge and the stagnation point on the cylinder, was similar in shape and position to our measured maximal convection heat transfer curve on the plate, see Fig. 9. The reason is not quite clear, but the maximum convection heat transfer may appear at the fluctuating (turbulent) free shear layer. Outside of this layer there is a laminar flow, and inside of the layer a low velocity turbulent flow is expected.

A sensitivity test was performed, in where the plate front edge was set to four different x- positions, in the range -1.0 $\leq xR^{-1} \leq$ 2.0, see Fig. 9. No significant variations were seen in the position of the minimum temperature curves relative to the cylinder. Other tests, at higher velocities, produced a less clear max convection heat transfer curve, probably because of spontaneous transition to turbulence, in the boundary layer on the plate.

In the present tests on the plate and at the lower velocity, the minimum temperature curves could therefore indicate the dimensions of the separated flow region, and the approximate position of the flow reattachment. It should be mentioned that this may also be the case for other separated flow regions.

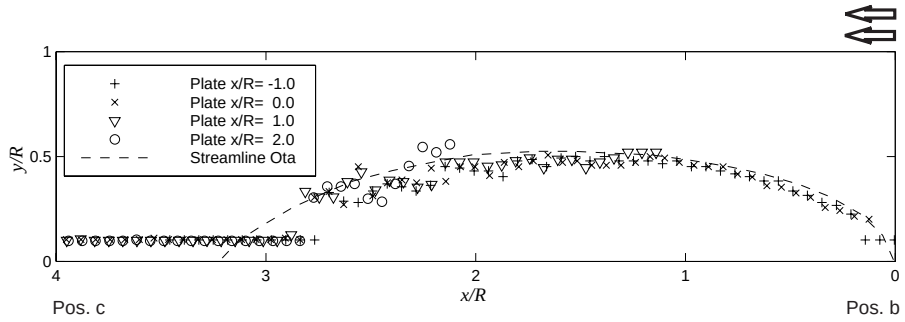

FIGURE 9. The minimum temperature curves found on the flow visualization plate, with the plate upstream edge positioned at different x- locations, for the cylinder in flow configuration (A) and $Re = 1.75 \times 10^5$. Included is a measured average dividing streamline at $Re = 5.62 \times 10^4$, Ota (1975).

Nu along the cylinder front surface a-b in configuration (A), was extrapolated (using the found local e and Eq. 10) to $Re = 4.2 \times 10^4$, used in the study by Sparrow & Geiger (1985), for comparison with their results, see Fig. 10. Our measured values is, at position (a), 10% lower, and near the corner the position b, 25 % lower than the data from Sparrow and Geiger. This trend of increasing difference is expected because of the different surface conditions used, Sparrow and Geiger used a surface of uniform naphthalene vapor density, which is analogous to a uniform wall temperature.

Along a constant heat flux surface for which Nu is increasing in the flow direction, the surface at a position downstream, will have a temperature lower than that of any upstream surface. The boundary layer flow is then warmer than it would be for a constant temperature surface, and Nu is therefore lower at the downstream position. The higher Nu seen at the center (pos. a) from Sparrow and Geiger, is in part expected from their higher free stream turbulence $Tu = 0.5\%$ compared to $Tu < 0.1$ % for the present measurements. The far extrapolation with Re is also a possible source of uncertainty.

configuration (A), was extrapolated to the lower $Re = 5.36 \times 10^4$ used by Ota & Kon (1977), using Eq. 10 with the local constant e, seen in Fig. 16. Ota and Kon performed the measurements on a long cylinder of $LD^{-1} = 13$ having a constant heat flux surface, and in a flow at $Tu = 0.8\%$. The comparison between their and our results is shown in Fig. 11. Nu is found to be in fair agreement, despite the 10-fold lower Re. The differences in cylinder length may not have an influence on Nu in this case, as was discussed above in relation to the size of separated region.

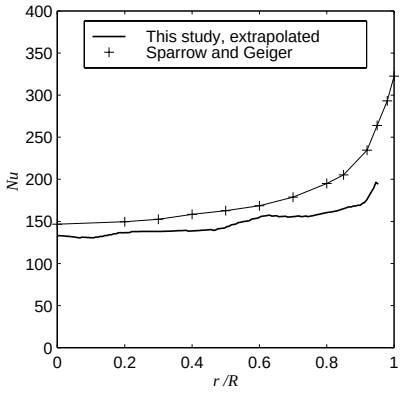

FIGURE 10. Nu along the cylinder front surface a-b in configuration (A), extrapolated, (using the local e and Eq. 10) of this study, to the Re =4.2×10^4 in the study by Sparrow and Geiger 1985, for comparison with their results.

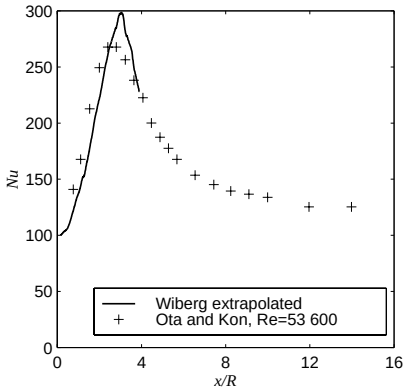

FIGURE 11. Nu along the cylinder surface b-c in configuration (A), extrapolated (using the found local e and Eq. 10) to the Re =5.36×10^4 in the study by Ota and Kon 1977, for comparison with their results.

The above described agreement between our results and those of Sparrow & Geiger (1985) Kiya et al. Kiya *et al.* (1991) and Ota (1975) and Ota & Kon (1977), also gives further credibility to the results.

4.2. *Measurements in configuration (B)*

A turbulence-generating grid was inserted upstream of the cylinder Fig. [1], generating a free stream turbulence intensity, Tu, of 6.7 %, and the experiments

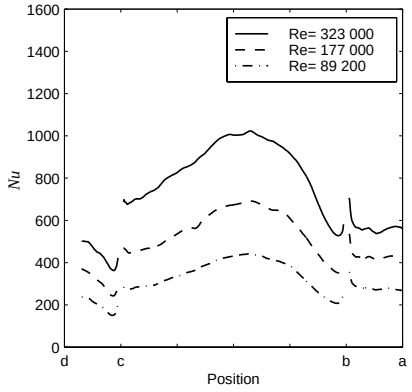

FIGURE 12. Nusselt numbers along the cylinder surface, from the measurements in axial flows with upstream turbulence Tu= 6.7 %, configuration (B), for different Re.

were conducted at Reynolds numbers of 3.23×10^5, 1.77×10^5, and 8.9×10^4. The Nusselt number distribution along the cylinder surface is shown in Fig. 12. Nu is seen to increase with Re, as expected, and the characteristic shape of the curves is similar for all Re.

On the front (upstream) surface of the cylinder, a-b, Nu maintains a nearly constant value, different for each Re. Compared with the results for $Tu < 0.1\%$ (Fig. 5), it shows that the increase of Tu to 6.7 % at Re= 3.23×10^5 caused this uniformity of Nu, as well as an increase of 42 % in the $\overline{Nu}_{a-b}$.

This increase in Nu due to the turbulence is similar in magnitude to that found by Lowery & Vachon (1975) on the front of a circular cylinder in cross flow. The results are consistent with the knowledge that increase in free stream turbulence both increases convective heat transfer coefficient magnitude and its uniformity.

The average $\overline{Nu}_{b-c}$, is significantly higher than on the front surface $\overline{Nu}_{a-b}$ and a maximum in Nu appear at xR^{-1}= 1.8. The flow reattachment, as determined by the tufts, appeared downstream of the maximum convection heat transfer and in between xR^{-1}= 2.00 and 2.26.

The temperature field on the flow visualization plate mounted above surface b-c, for this configuration (B) is shown in Fig. 13. The dimension of the separated region is here indicated smaller than it was for the cylinder in configuration (A), and the curve of minimum temperature had a maximal height of yR^{-1}= 0.3 at about xR^{-1}= 1, aiming towards the cylinder surface at about xR^{-1}= 2, which agree with the position of the mean flow reattachment as measured using the tufts.

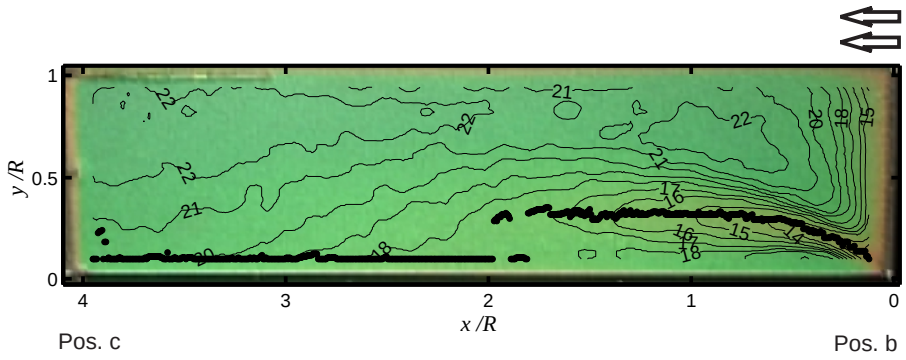

FIGURE 13. Isotherms, $T - T_\infty$, on the flow visualization plate mounted above the cylinder in configuration (B), Re= 1.75×10^5, Tu= 6.7%. The minimal temperatures are marked with black dots.

On the rear surface c-d, Nu drops to a lower value, increasing from the cylinder edge towards its center. Along the whole surface a-b-c-d, the average for these three Reynolds numbers (3.23×10^5 , 1.77×10^5 and 8.9×10^4) was found to be $\overline{Nu}_{a-d}$= 780, 520 and 330, respectively.

4.3. *Measurements in configuration (C).*

A disk with diameter 1/3 D was placed upstream of the cylinder as detailed earlier for configuration (C), and measurements were performed on the cylinder at Reynolds numbers of Re= 6.09×10^5 , 3.23×10^5 and 1.77×10^5, at $Tu < 0.1\%$. The Nusselt number distribution along the cylinder surface is shown in Fig. 14 a, in where Nu is seen to increase with Re, as expected, and the characteristic shape of the curves is similar for all Re.

On the front (upstream) surface of the cylinder, a-b, Nu increases from the cylinder center to its edge. On the surface b-c, a sharp maximum in Nu appear close to its upstream (front) edge, with Nu decreasing to about half of the maximal value towards the rear edge.

The temperature field on the flow visualization plate mounted above surface b-c, for this configuration (C) is shown in Fig. 15. The curve of minimum temperature, which was seen both in configurations (A) and (B), can not be seen here, indicating a much smaller or non existing separated region. A growing region of high convection heat transfer towards its rear can be seen on the plate, possibly related to growing turbulent flow structures along the cylinder.

On the rear surface c-d, Nu is lower, increasing from the cylinder edge towards its center. The average Nusselt number along the entire surface a-b-c-d, was for these three Re found to be $\overline{Nu}_{a-d}$= 1220, 790 and 490, respectively. Moving the disc closer to the cylinder, from 1.00 D to 0.50 D from front

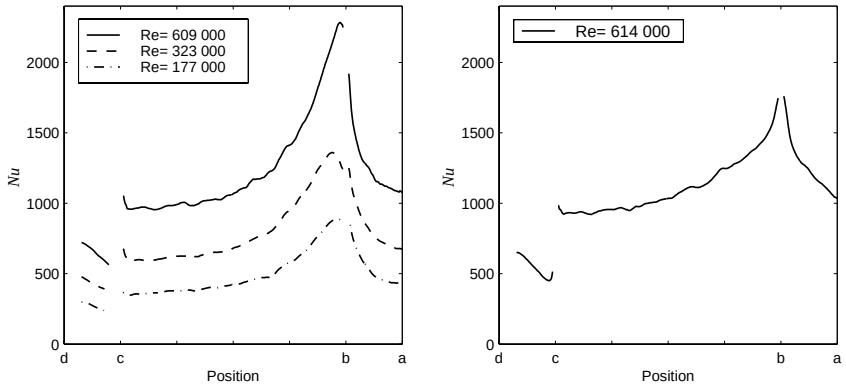

FIGURE 14. Nu along the cylinder surface for different Re. (a), with a 1/3 D diameter disk placed 1.00 D upstream of the cylinder in configuration C. (b), with a 2/3 D diameter disk placed 1.00 D upstream of the cylinder in configuration (D).

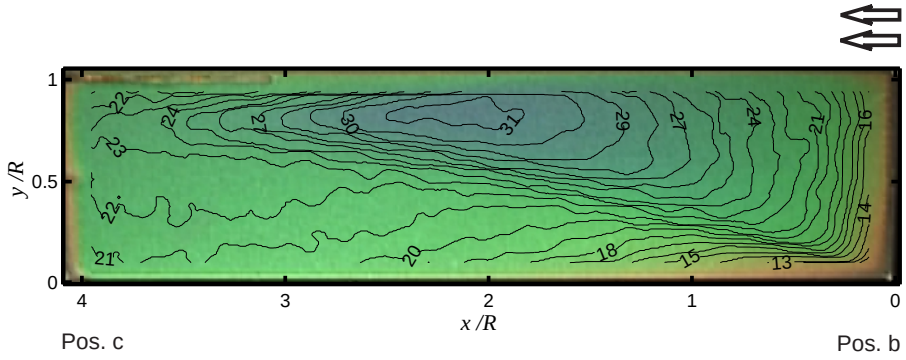

FIGURE 15. Isotherms, $T - T_\infty$, on the flow visualization plate mounted above the cylinder in configuration (C), Re= 1.75×10^5, $Tu < 0.1\%$ upstream of the disc. The minimal temperatures are marked with black dots.

surface, gave asymmetric values of Nu on the front surface a-b, and symmetry was re-established when its distance was again increased to 1.00 D. The drag coefficient, for the disc and the cylinder front together, is expected to change from 0.72 while the disc is absent, to 0.28, using the disc in configuration (C). Estimated from the measurements by Koenig & Roshko (1985).

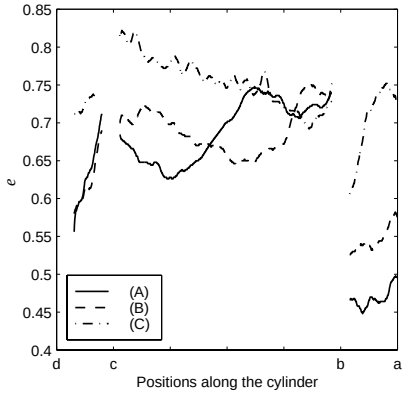

FIGURE 16. The calculated local exponents e of eq. 9 along the cylinder surfaces, for the flow configurations (A), (B) and (C).

4.4. *Measurements in configuration (D)*

Here a disc twice as large as the previous one, of diameter $2/3\ D$, was placed upstream of the cylinder as detailed earlier for configuration (D), for Re= 6.14×10^5 . As shown in Fig. 14 b, Nu is similar to that in configuration (C) at the same Re level. The main difference is the peak in Nu at the front edge (pos. b), which is lower, further confirmed by the lower $\overline{Nu}_{a-d}$= 1080.

On the downstream surface c-d Nu was found to be very similar to Nu in the configurations (A), (B), (C), which indicated a low sensitivity in Nu to the different upstream flow conditions in the wake region.

The drag coefficient, for the disc and the cylinder front together, is expected to change from 0.72 while the disc is absent, to 0.2, using the disc in configuration (D), estimated from the measurements by Koenig & Roshko (1985).

4.5. *The dependence of Nu on Re.*

The observed similarity of the curves which describe the dependence of Nu on Re for all Reynolds numbers investigated here, Figs. 5, 8, 10, indicates that it may be possible to find a value of the power e that would describe the behavior of the local Nu with respect to Re as is shown in Eq. 9. These values, for all cylinder surfaces for the configurations (A), (B) and (C), were calculated and are shown in Fig. 16.

On the front surface a-b, and for configurations (A) and (B) it was found that e increased with an increase in Tu , while e was even larger when measured using the disc in configuration (C).

Conf.		a-b	b-c	c-d	a-d
(A)	C	1.088	0.122	0.096	0.134
	e	0.466	0.682	0.656	0.668
(B)	C	0.662	0.140	0.140	0.155
	e	0.534	0.686	0.632	0.674
(C)	C	0.162	0.058	0.055	0.070
	e	0.678	0.750	0.704	0.734

TABLE 1. The constants C and e of eq. (9) for the averages $\overline{Nu}_{a-b}$, $\overline{Nu}_{b-c}$, $\overline{Nu}_{c-d}$ and $\overline{Nu}_{a-d}$ and for the flow configurations (A), (B), and (C).

On the middle surface b-c, e had a minimum where Nu has a maximum. For configuration (A) the minimum in e was found at xR^{-1}= 3.0, for configuration (B) it was at xR^{-1}= 1.8, and for configuration (C) at xR^{-1}= 0.55. For all the configurations, e was found to increase with a similar slope from the minimum and towards pos. c.

It is noteworthy that Ota & Kon (1977), were able to collapse their results, which were measured at lower Re numbers, (see the introduction for details), all along their much longer cylinder, using the exponent e= 0.75.

On the rear surface c-d, for each of the configurations, e was somewhat lower than on the middle surface b-c, decreasing from the edge.

Nu were averaged, and C and e for the averages of Nu on surface a-b, b-c, c-d and the whole cylinder a-d, and for the three configurations (A), (B), (C), can be seen in Table 1. The exponent, which indicate the trends with Re, based on the averages for the whole cylinder and for all the configurations (A), (B), (C), was found in the range $0.67 < e_{a-d} < 0.73$.

I all these cases, most of the cylinder surface were within, the separated, the reattached or within the wake region (in the rear wake, or in the wake behind the discs, in configurations (C) and (D)). Only for configuration (A) and for the front surface a-b, which occupy 11 % of the total surface, a laminar boundary layer flow was expected, and the exponent was there found at its lowest level, e_{a-b}= 0.46.

4.6. *An example of practical consequences for axial flow gas cooling of an LD^{-1} =2 cylinder*

As stated in the introduction, gas quenching of steel is improved with the magnitude and uniformity of the convection heat transfer coefficients (h). A comparison between the configurations (A), (B), (C) and (D) was performed, for a representative example: nitrogen gas quenchant at 10 bar, 300 K and a flow velocity of 20 ms^{-1}. A cylinder of 49 mm diameter will produce for this flow a Re= 6.14×10^5 .

Config.	$\overline{Nu}_{a-d}$	$\overline{h}_{a-d}$ $\mathrm{Wm^{-1}K^{-1}}$	σ_{Nu}	σ_{max}
(A)	990	540	0.32	0.89
(B)	1240	680	0.24	0.78
(C)	1240	680	0.31	1.42
(D)	1080	590	0.24	1.2

TABLE 2. The averages $\overline{Nu}_{a-d}$ and $\overline{h}_{a-d}$ and their nouniformities for a typical gas quenching case of a 49 mm dia., 98 mm long cylinder in 20 $\mathrm{ms^{-1}}$ axial flow of nitrogen quenchant at 10 bar, 300 K

The average $\overline{Nu}_{a-d}$ were calculated using eq. 9, with the coefficients C and e found in this study (Table 1). $\overline{h}_{a-d}$ was then evaluated from eq. 4 and the results are presented in table 2. For this comparison, Nu were for configurations (B) extrapolated to the higher Re of interest. The coefficient $\overline{h}_{a-d}$ was in configuration (B) found to be 25 %, in (C) 26 %, and in (D) 10 % higher than in configuration (A) with the un-affected free stream.

The non-uniformity in Nu (and h) σ_{Nu} was found, compared to configuration (A), lowered by 26 % in configuration (B), by 26% in configuration (D), by very little in configuration (C). The second non-uniformity number σ_{max} confirms that configuration (B) has the lowest non-uniformity in Nu.

Therefore, the configuration (B) generated the highest average $\overline{h}_{a-d}$ at also a low non-uniformity σ_{Nu} and σ_{max}, and may therefore be the best choice for quenching. The upstream turbulence generation grid will generate an undesirable pressure drop, but a possible solution to this problem could be to use a grid, or another smaller device for disturbing the flow locally in front of the cylinder, which can generate a similar effect at a lower pressure drop. It should also be noted that high levels of upstream turbulence will exist anyway in commercial quench chambers, due to effects of the fan and the flow geometry.

5. Conclusions

The local Nusselt number (Nu) distributions on all surfaces of a two-diameter long cylinder was measured in axial flows of air, at Reynolds numbers (Re) of 8.9×10^4 to 6.17×10^5 (9 to 63 $\mathrm{ms^{-1}}$), by using thermochromic liquid crystals (TLC) on thin foils which produced a constant surface heat flux.

Different upstream air flow conditions were examined, and set by varying the flow turbulence level (Tu) by the use of a turbulence generating grid, and by using flow modification inserts that were circular discs of two sizes, in front of the cylinder. These and the grid were found to create a major change in the magnitude and distribution of the local Nu on the cylinder.

Nu was found to increase with the Re, but at different amounts for different locations on the cylinder. Correlations in the form $Nu = CRe^e$ were developed and presented for the three different cylinder surfaces $\overline{Nu}_{a-b}$, $\overline{Nu}_{b-c}$, $\overline{Nu}_{c-d}$ and for the whole cylinder, $\overline{Nu}_{a-d}$, and for the local values along the cylinder.

Increase of the turbulence intensity (Tu) from <0.1% to 6.7% at the same Re= 6.14×10^5, increased the average Nusselt number over the cylinder by 25%, and decreased the Nu non-uniformity's (σ_{Nu} and σ_{max}) by 26% and 12%, respectively. For the same Re the largest flow modification insert (a circular disc in front of the cylinder) increased $\overline{Nu}_{a-d}$ by 10 % and reduced σ_{Nu}, by up to 25% but increased σ_{max} by 33 %.

A TLC-coated heated flat plate mounted in the flow above the cylinder was demonstrated to help visualize the flow field above the cylinder: The temperature field on the plate was affected by the flow, and a track of minimal temperatures (maximal h) appeared on the plate, which was shown to be the same as the envelope of the separated flow region above the cylinder, i.e. the dividing stream line.

The location of flow reattachment on the cylinder curved surface was measured using tufts, and was for configuration (A) found similar to the location of the maximum in Nu. For configuration (B) the maximum in Nu was found within the separated region.

Our results agree well with the small amount of data published by others, when extrapolated to their conditions.

6. Acknowledgments

This work was partially supported by AGA AB (now Linde Gas) and Ipsen International GmbH. Marcus Gällstedt and Ulf Landen is acknowledged for valuable help with the experimental equipment. Ulf Andersson at Calesco foil AB is acknowledged for his constructive cooperation in the design and manufacturing of the foil.

References

Achenbach, E. 1975 Total and local heat transfer from a smooth circular cylinder in cross-flow at high reynolds number. *Int. J. of Heat and Mass Transfer* **18**, 1387–1396.

Achenbach, E. 1989 Heat transfer from a staggered tube bundle in cross-flow at high reynolds numbers. *Int. J. of Heat and Mass Transfer* **32** (2), 271–280.

Ferrari, J., Lior, N. & Slycke, J. 2003 An evaluation of gas quenching of steel rings by multiple-jet impingement. *J. Materials Processing Technol.* **136**, 190–201.

Kiya, M., Mochizuki, O., Tamura, H., Nozawa, T., Ishikawa, R. & Kushioka, K. 1991 Turbulence properties of an axisymmetric separation-and-reattaching flow. *AIAA Journal* **29** (6), 936–941.

Koenig, K. & Roshko, A. 1985 An experimental-study of geometrical effects on the drag and flow field of 2 bluff-bodies separated by a gap. *J. Fluid Mech.* **156**, 167–204.

Lind, M., Lior, N., Alavyoon, F. & Bark, F. 1998 Flows effects and modeling in gas-cooled quenching. In *Proc. Heat Transfer 1998, 11th International Heat Transfer Conference, Kyongju, Korea*, , vol. 3, pp. 171–176.

Lindgren, B. & Johansson, A. V. 2002 Evaluation of the flow quality in the mtl wind-tunnel. Technical report TRITA-MEK report 2002:13. Dept. of mechanics, KTH.

Lior, N. 2003 The cooling process in gas quenching, invited keynote presentation and paper. In *Proc. International Conference on Advances in Materials and Processing Technology, AMPT 2003, Dublin, Ireland*, , vol. 1, pp. 171–179.

Lowery, G. W. & Vachon, R. I. 1975 The effect of turbulence on heat transfer from heated cylinders. *Int. J. of Heat and Mass Transfer* **18**, 1229– 1242.

Ota, T. 1975 An axisymmetric separated and reattached flow on a longitudinal blunt circular cylinder. *J. of Applied Mechanics* pp. 311– 314.

Ota, T. & Kon, N. 1977 Heat transfer in an axisymmetric separated and reattached flow over a longitudinal blunt circular cylinder. *J. of Heat Transfer* pp. 155– 157.

Sparrow, E. M. & Geiger, G. T. 1985 Local and average heat-transfer characteristics for a disk situated perpendicular to a uniform-flow. *J. of heat transfer-transactions of the asme* **107** (2), 321–326.

Thuvander, A., Melander, A., Lind, M., Lior, N. & Bark, F. 1999 Prediction of convective heat transfer coefficients and their effects on distortion and mechanical properties of cylindrical steel bodies quenched by gas cooling. In *paper AJTE99-6289 in 5th ASME/JSME Joint Thermal Engineering Conference, San Diego*, pp. 171–176.

Vynnycky, M., Ferrari, J. & Lior, N. 2003 Some analytical and numerical solutions to inverse problems applied to phase-transformation tracking gas quenching. *ASME J. Heat Transfer* **125** (1), 1–10.

Wiberg, R. & Lior, N. 2003 Error causes and magnitudes in thermochromic liquid crystals thermometry, paper imece2003-42101. In *IMECE'03, 2003 ASME International Mechanical Engineering Congress & Exposition Washington, D.C., USA*, pp. 15–21.

Wiberg, R., Muhammad-Klingmann, B., Ferrari, J. & Lior, N. 2000 Use of thermochromic coatings for the experimental determination of the distribution of heat transfer coefficients in gas-cooled quenching. In *Proc. 5th ASM Heat Transfer and Surface Eng. Conf. in Europe., Gothenburg, Sweden*, pp. 275–286.

Zdravkovic, M. M., ed. 1997 *Flow around circular cylinders, vol. 1 Fundamentals*. Oxford science publications, Oxford University Press Inc.: Oxford.

Zdravkovic, M. M., ed. 2003 *Flow around circular cylinders, vol. 2 Applications*. Oxford science publications, Oxford University Press Inc., New York.

Zukauskas, A. 1989 *High-performance single-phase heat exchangers*. Hemisphere Pub., New York.

Zukauskas, A. & Ziugzda, J., ed. 1985 *Heat Transfer of a cylinder in Crossflow*. Springer- Verlag, Berlin.

Paper 3

P3

Heat transfer from quadratic prisms in cross flow

By Roland Wiberg[⋆] A. Stroppiana [⋆] and Noam Lior[⋆⋆]

[⋆]FaxénLaboratoriet, Dept. of Mechanics, KTH, SE-100 44 Stockholm, Sweden
Email: roland@mech.kth.se
[⋆⋆]Dept. of Mechanical Engineering and Applied Mechanics, University of Pennsylvania, Philadelphia, PA 19104-6315, U.S.A.

To be submitted

Experimental investigations on the local and average heat transfer from a square prism, with an edge facing the flow, and from two prisms arranged in-line at different distances, and from four prisms arranged in a square pattern, were carried out in cross flows of air at Reynolds numbers $2.9\times10^4 < Re < 1.39\times10^5$. Thermochromic liquid crystals (TLC) and thin foils, were used for these measurements and particle image velocimetry (PIV) was used for flow velocity measurements. A splitter plate behind the single prism killed the vortex shedding and halved the average Nusselt number Nu on the downstream side. For the two prisms arranged in-line, Nu showed three main different distributions appearing in three different intervals of distance, and the flow was found to be unstable and intermittently switching, in the interval 5.83 to 6.67 side lengths between the prisms. The largest values in Nu appeared for distances 1.66 to 2.00 side lengths apart.

Key words: flow across bluff bodies, convective heat transfer, quadratic prisms, flow visualization, particle image velocimetry, thermochromic liquid crystals

1. Nomenclature

D: side length of the prism.
h: local convection heat transfer coeff., $\mathrm{Wm^{-2}K^{-1}}$.
k_∞: heat conductivity of the upstream air, $\mathrm{Wm^{-1}K^{-1}}$.
L: length of the prism.
Nu: local Nusselts number, dimensionless.
$\overline{Nu}$: surface average of Nu, dimensionless.
Re: Reynolds number, dimensionless.
p: distance between the centers of the prisms. s: coordinate along the prism surface.
T: local surface temperature.
T_∞: upstream air temperature.
TLC: Thermochromic Liquid Crystals.
Tu: u'_{rms}/U_∞, free stream turbulence, dimensionless.
U_∞: upstream time-averaged air velocity.
u': upstream fluctuating air velocity.
q'': electrically supplied surface heat flux, $\mathrm{Wm^{-2}}$.

1.1. *Greek symbols*

α: angle of attack for the prism.

2. Introduction

In the course of our studies on the relatively new method of using fast-flowing high pressure gases for the rapid cooling of single or multiple steel parts for their hardening, (cf. Lind *et al.* (1998), Lior (2003), it was found that little information is available on the distribution of the convective heat transfer coefficients over the surfaces of the cooled parts for the pertinent Reynolds numbers (Re) which typically are above 10^5 and often above 10^6.

This study investigates experimentally the flow and consequent convective heat transfer over the surfaces of single and multiple quadratic-cross section prisms (bars) at attack angle $\alpha = 45°$ (Fig. 1) for the following configurations: 1) a single prism with and without a downstream splitter plate, 2) two in-line prisms at varying distances apart, and 3) four prisms in a square pattern. A prism was chosen in this study because of the expected lower sensitivity of the nature of the flow to the Reynolds number, as opposed to circular cylinders which exhibit many different types of flow patterns depending on the Reynolds number, Zdravkovic (1997).

For a single prism in cross flow at $\alpha = 45°$ and the Reynolds numbers in this study, one can consistently expect laminar flow in the boundary layers for the accelerating flow above the two upstream surfaces, separation from the surfaces

at the top (middle) corner, and a turbulent wake above the two downstream surfaces.

The flow around a single quadratic prism, in cross flow at different angles of attack $0 < \alpha < 45°$ was investigated, Igarashi (1984*a*). Using smoke visualization, pressure, drag and vortex shedding frequency measurements and for $3.85 \times 10^3 < Re < 7.7 \times 10^4$ and Tu= 0.5%. Four different flow regimes were detected, 1) $0 \leq \alpha \leq 5°$: perfect separation type, symmetric flow, 2) $5 < \alpha \leq 13°$: perfect separation type, unsymmetrical flow, 3) $14 < \alpha \leq 35°$: reattachment flow type, a separation bubble exists on the lower surface, 4) $35 < \alpha \leq 45°$: wedge flow type.

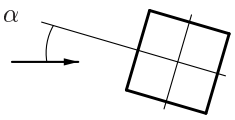

FIGURE 1. A quadratic prism at different angles of attack α, to the incoming flow.

The smallest drag force, and at the same time the largest lift force, appeared for the angles $13 < \alpha < 14°$, while the largest drag force appeared for $\alpha = 45°$. In another investigation, at $Re = 1.76 \times 10^5$ and 0.5%$< Tu <$12.5% and for $0 < \alpha < 45°$, the Strouhal number (based on the prism side length), was found in the range 0.115 to 0.145, Lee (1975). The largest frequency was found at the angle were the drag force had a minimum, which was thought to be associated with a minimum wake width.

The convection heat transfer parameter Nu on a square prism and at different angles of attack were investigated, for $5.6 \times 10^3 < Re < 5.6 \times 10^4$ and Tu= 0.5%, Igarashi (1985). The surface averaged Nu had a minimum at the angle $\alpha = 12°$, while a maximum was found for $20 < \alpha < 25°$. No differences were detected in the average of Nu, between the two cases; a constant surface temperature, and at constant surface heat flux.

For the flat downstream surface of different bluff bodies, 1) a prism ($\alpha = 0°$), 2) a semi circular cylinder, 3) an equilateral triangular prism, 4) a flat plate perpendicular to the flow, the local Nu values were found to be almost constant over the surfaces and similar in magnitude, Igarashi (1986). The surface averaged Nu in the separated regions was found to be correlated to Re as,

$$\overline{Nu} = 0.17Re^{2/3}$$

when using this relation for the separated region of a prism in wedge flow ($\alpha = 45°$), the constant 0.17 is replaced with 0.145. For the upstream surfaces at $\alpha = 45°$ the correlation was found to be,

$$\overline{Nu} = 0.72Re^{1/2}$$

An investigation on how to relate the drag coefficient to wake parameters, such as the base pressure of different type of bluff bodies was performed, Roshko (1955). Measurements of the Strouhal number of a circular cylinder with a short downstream splitter plate, at different gaps between the cylinder and the plate were also performed. A conclusion was that the critical region for the formation of the whole flow field around a bluff body, is found within 4-5 diameters behind the body. A plate length of 7 to 10 diameters, depending on cylinder cross-section shape is sufficiently long for the near wake to be independent of that length, Roshko (1993).

A short splitter plate was inserted downstream of a circular cylinder. Nu on the upstream non-separated region was not affected for varying gaps between the plate and the cylinder, while large changes was seen in the separated region, Igarashi (1984*c*). For an optimal gap the convection heat transfer could be halved, compared to a cylinder without the plate, while for an other gap, a small increase was seen in the rear part.

No investigations have been found in the literature on the convection heat transfer coefficients for two quadratic prisms arranged in-line at the angle of attack $\alpha = 45°$, which is one of the configurations investigated in this report. The closest to that are several investigations on the flow around two prisms arranged in-line at angle of attack $\alpha = 0°$ and on circular cylinders arranged in-line. Such results will serve as an introduction for the present investigation.

The flow around two circular cylinders of the same diameter d in cross flow at distances apart $1.03 < p/d < 5.0$, was investigated using smoke visualization, surface pressure and wake frequency measurements, for $8.7 \times 10^3 < Re < 5.2 \times 10^4$ and $Tu = 0.55\%$, Igarashi (1981). Six different flow patterns were detected, as the distance p between the cylinder centers was changed in that range, which is shown in Fig. 2,

Pattern A: The separated shear layer from the upstream cylinder does not reattach onto the downstream cylinder, $(1.0 < p/d < 1.1)$. Pattern B: the shear layer reattach onto the downstream cylinder, $(1.1 < p/d < 1.6)$. Pattern C: quasi-stationary vortices are formed between the cylinders, $(1.6 < p/d < 2.3)$.

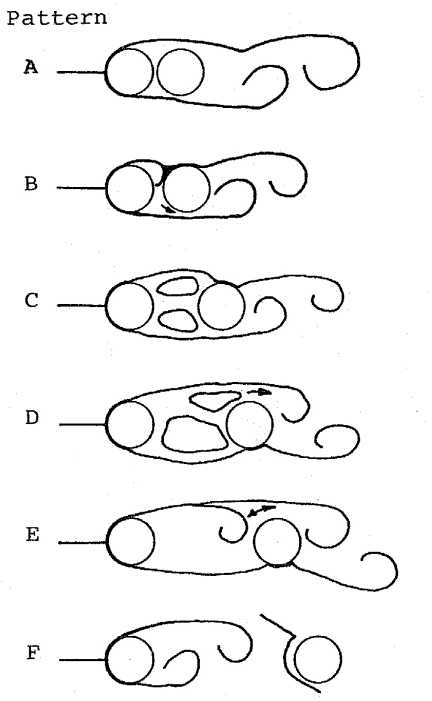

FIGURE 2. Sketch of flow patterns around two circular cylinders arranged in-line, Igarashi (1981).

Pattern D: vortex shedding detected intermittently, $(2.3 < p/d < 3.1)$. Pattern E: bi-stable flow, the shear layer rolls up in front of the cylinder intermittently, $(3.1 < p/d < 3.75)$. Pattern F: the shear layer rolls up in front of the cylinder, $(p/d > 3.75)$. This description are given for $Re > 3.5 \times 10^4$, somewhat different behavior was seen for lower Re.

For pattern B flow was passing between the cylinders across the center line, synchronized with the vortex shedding, Igarashi (1984*b*). For patterns B, C, D, the shear layer from the upstream cylinder reattach onto the down stream cylinder at 60° to 70°, measured from the cylinder front. For pattern E two different flow types exist and are intermittently switching (bi-stable flow). One of the flow types is more stable than the other, dependent on the distance between the cylinders. The drag force for the two cylinders together decrease ca 60%, when the flow change from pattern F to pattern D . For pattern F, the pressure distribution on the upstream cylinder was found similar to that of a single cylinder, indicating that the flow around the cylinder was independent of the presence of downstream cylinder.

The effects of small scale free stream turbulence on the flow around two tubes arranged in-line was investigated, for $Re = 2.0 \times 10^4$, Tu=0.1, 1.4 and 3.2% and $1.25 < p/d < 5.0$, Ljungkrona *et al.* (1991). The free stream turbulence had a strong influence on the flow, and the critical spacing was found to decrease from p/d= 3.5 to 2.5, as the turbulence intensity was increased from 0.1% to 1.4%. The Strouhal number, changed as most from 0.24 to 0.14. A further increase to Tu= 3.2%, had a small influence. For distances larger than the critical spacing, the effects of Tu were found small.

3. The experimental technique

The measurement of the convective heat transfer coefficient distribution on the prism surfaces was performed by electrically applying a constant known heat flux to a thin foil, and measuring the free stream air temperature and the surface temperature distribution on the foil, the latter using thermochromic liquid crystals (TLC). These crystals change their color with temperature, and digital video photographs of the TLC were translated to temperatures by image processing software developed by us for this purpose, and more details about this technique and its accuracy can be found in Wiberg & Lior (2003). More information about this measurement is given further below.

The experiments were performed in a closed circuit wind tunnel at the Department of Mechanics at KTH, the free stream turbulence level in an empty test section is within Tu = 0.04 %, (for further information about the wind tunnel see Lindgren & Johansson (2002)). The test section had a constant flow cross-section (Fig. 3). At the end of the test section there is an opening slit to the surrounding, to equalize the pressure with the atmosphere. The roof and the floor of the test section were made of 20 mm thick Plexiglas, which allowed visual access from outside. A control system fixed the air temperature during the measurements to between 22°C and 30°C and the upstream flow velocities were fixed at values between 7 to 36 m/s. The prism surface temperature were within the active range of the thermochromic liquid crystals (TLC), 36°C to 63°C.

3.1. *Determination of the convective heat transfer coefficient (h).*

The convective heat transfer coefficient (h) was determined from Eq. 1, where the electrically supplied heat flux q'', the prism surface temperature field T, and the upstream air temperature T_∞ were measured. The local convective heat flux from the cylinder surface is the electrically supplied heat flux q'' reduced by the local radiative heat flux calculated as shown in Eq. 1, with emittance assumed to be equal to 1 because the surface is black. The surface averaged radiative flux was typically 5 -15 % of q'', with the lower values for the higher Re.

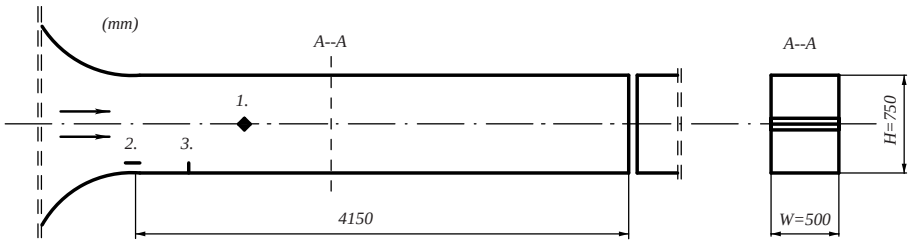

FIGURE 3. The test section. 1. the studied prism 2. The Prandtl tube for the free stream velocity measurement, 3. the thermocouple for air temperature measurement.

$$h = \frac{q'' - 5.67 \times 10^{-}8(T^4 - T_\infty^4)}{T - T_\infty} \tag{1}$$

T was measured using the thermochromic liquid crystal (TLC) technique, as described in more detail below.

3.2. *The test prism (Fig. 5) and its surface temperature measurement.*

The square-cross-section test prism was built to also produce a constant surface heat flux surface during the measurements. A square aluminum bar 20×20 mm, was used at the center to give the model rigidity and, indeed, no vibrations were observed visually during the measurements. Insulating extruded polystyrene (EPS, density 40 Kg/m^3, heat conductivity 0.033 W/mK) 20 mm thick was applied to the aluminum surfaces. Four T-type thermocouples were installed to the prism axis in the EPS surface, using epoxy glue. The first in the middle of one side, and the other three on the opposite side of the prism, one in the middle of the side, and the two other 10 mm from the edges, with a length of 120 mm beneath the heated foil along the prism axis. The thermocouples were calibrated in an isothermal bath and their accuracy was determined to be $\pm 0.2^\circ$ C. A 125 μm polyester foil ($k = 0.13$ W/mK) was glued to the outer surfaces of the EPS to make it smooth.

The constant heat flux was produced by a resistor-embedded foil bonded on top of the polyester foil. The former foil was designed by us for this purpose and manufactured by Calesco Foil AB, [1] where the resistors are 12 μm thick 1.5 mm wide strips of Inconel (k= 12 $W/(m^\circ C)$, with low temperature-dependency resistance coefficient of 1.25 $\times 10^{-4}$ $1/^\circ C$), spaced 0.2 mm apart and embedded in a 50 μm thick Kapton (polyimid) plastic (k= 0.12 $W/(m^\circ C)$, max temp.

[1]Calesco Foil AB Västeråsvägen 9 S-73040 Kolbäck Sweden

400°C)) (Fig. 4). This design made the heat flux adequately uniform over the entire foil surface for this purpose. The electrical resistance uniformity of the metallic foil was measured to be ± 1 % of the surface average. The metallic foil was divided into 7 zones, connected in parallel to variable voltage 0- 240 V a.c. transformer, which supplied a tension and current to the foil, giving a power to the foil measured to be constant within ± 1.5 %.

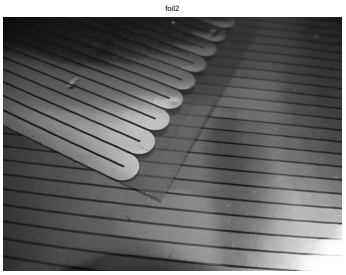

FIGURE 4. The heating foil.

Black paint was sprayed on the whole metallic foil, and the Hallcrest[2] micro-encapsulated TLC of type C17-10 R35C20W was then sprayed in a few thin layers to form a uniform film with a thickness estimated to be 20 μm. Additional quadratic prisms of the same dimensions as the heated prism were made of aluminum for the experiments using multiple prisms. The corners of all the prisms had a estimated precision or radius of 0.2 mm.

[2]Hallcrest 20 Downing Road, West Meadows Industrial Estate, Derby, UK, DE21 6HA.

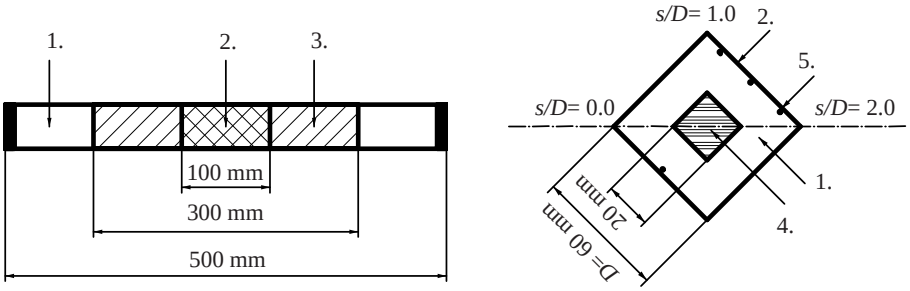

FIGURE 5. The test prism used for the convection heat transfer measurements. Left figure, prism long surface view. Right figure, prism cross section. 1. the thermal insulation, EPS , 2. TLC on the heating foil, 3. foil without TLC, 4. the aluminum core, 5. thermocouples. s, variable along the surface.

3.3. *The measured flow configurations*

The measurements on the prisms, all at $\alpha = 45°$ (Fig. 1), were performed in cross flow in four configurations, shown in Fig. 6. Configuration A) a single prism, B) a single prism with a thin plate (splitter plate) mounted downstream, C) two prisms arranged in-line at different distances between the centers, $1.45 < p/D < 8.00$. D) four prisms mounted in a square pattern. The flow blockage in the wind tunnel for configuration A, B and C was $2^{1/2}D/H = 0.11$ and for configuration D$= 0.22$, the length to side length ratio $L/D = 8.33$. These figures imply a small influence on the flow, while in configuration D it may have an influence, however, no corrections for tunnel blockage was done.

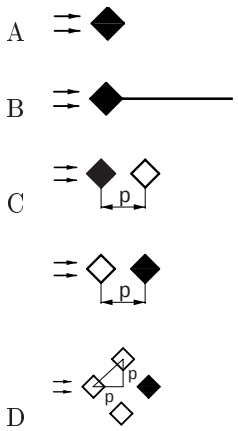

FIGURE 6. The configurations used for the measurements, black prisms were heated and TLC-measured, and white prisms were not.

The splitter plate used in configuration B was of the same width W as the test section and 300 mm long, with its leading edge 2 mm downstream of the rear corner of the prism. It was made of 2 mm thick aluminum and was fixed to the test section walls, and by six 1 mm supporting wires along its center line, which prevented vibrations. Special attention was given in all configurations to make the prism center line (Fig. 5) parallel to the test section floor and roof.

Color photographs of the TLC were taken through the wind tunnel Plexiglas window from a fixed position outside the test section, and special attention was paid to shield any light reflections and optical disturbances. A Sony DCR-TRV 900E camera, 680×510 pixels and 3×8 bits color resolution, and a 24^o 50 W halogen lamp fixed to the camera, were used to take the TLC surface pictures. Using Fire wire (IEEE- 1394), the photography digital signals were

transferred from the camera to a Macintosh computer QuickTime program, and further into the Matlab5.2.1^{TM} [3] program *rgb2hsv* that computes the color variable called hue. A functional relation between that hue and the temperature measured by thermocouples obtained by in-situ calibration was then used to calculate the Ts field. Further details about this TLC technique and its accuracy are available in Wiberg & Lior (2003).

3.4. *Calibration of the TLC.*

The TLC was calibrated in-situ on the prism and inside the test section, using the thermocouples in the surface as the reference. Possible effects of aging of the TLC were taken into account by interpolating between the calibrations performed before and after the measurements. The possible effects of TLC nonuniformities were tested in-situ by keeping the prism nearly isothermal by heating and mixing the air in test section to a test temperature level for which the TLC has the largest sensitivity to disturbances. Based on our calibrations, the estimated total errors in the TLC measured temperatures were within ± 1 °C.

3.5. *The experimental procedure*

Before a measurement, the upstream flow velocity U_∞, measured using a Prandtl tube, and the upstream flow temperature T_∞, measured using a thermocouple, were allowed to stabilize, (U_∞ estimated within ± 0.5% and T_∞ ± 0.2°C). The surface heat flux q'' of the foil, measured using voltage and current meters, was then increased until the surface temperatures came within the active interval of the TLC color play. The prism surface temperatures were then allowed to stabilize within ± 0.3°C, as indicated by the thermocouples, for typically over 10 minutes.

In this steady state, color photographs of all the four sides of the prism were captured, using the same camera settings, view angle and light, as were used during the in-situ calibrations. The electrical power supply to the foil was then shut off.

The thermocouples were read and viewed by a computer, which also was used to automatically shut off the electric power if the surface temperatures exceeded a fixed level, chosen to be near the upper limit of the TLC.

3.6. *Data analysis*

For each side of the prism the measured color values were averaged over the length of the TLC coated area, giving just one value for each position s, totally 400 s-dependent temperature values for each side. The colors were then translated into the surface temperature field T as described earlier.

[3] The MathWorks, 3 Apple Hill Drive, Natick, MA 01760-2098

The convective heat transfer coefficient, h, was calculated using Eq. 1, and expressed in terms of the Nusselt number, Nu (dimensionless), using

$$Nu = \frac{hD}{k_\infty} \tag{2}$$

where D is the length of a side of the prism, and k_∞ is the heat conductivity of the upstream air. Nu was then averaged over the prism to give only one Nu for each s-position. Surface averages of $Nu(s)$ were calculated, over, 1) the upstream surfaces $\overline{Nu}_{0-1}$, 2) the downstream surfaces $\overline{Nu}_{1-2}$, and 3) the whole prism $\overline{Nu}_{0-2}$.

The Reynolds number (Re) for the flow over the prism, is defined by Eq. 3, where ν_∞ was the kinematic viscosity of the upstream air and D the side length of the prism.

$$Re = \frac{U_\infty D}{\nu_\infty} \tag{3}$$

As commonly done for such flows, Nu was correlated with the Reynolds number Re as

$$Nu = CRe^e \tag{4}$$

where C and e were unknown constants to be determined from the measurements. Nu was measured at different Re levels, and C and e were calculated by finding the value of e which minimized the relative differences in the calculated coefficient C.

3.7. *Errors evaluation*

To estimate the symmetry in the data over the prism, measured surface temperatures on the four sides of the prism, and for three different configurations A, B and C, are shown in Fig. 7. The differences seen in the data over the prism, which was rotated to $\alpha = 45^o$, indicates in each of the configurations the level of symmetry, which was within the range of errors for the method.

A comparison of our heat transfer results measured in configuration (A) with those from Igarashi (1986) is shown in Fig. 8. Igarashi used a constant heat flux surface and Re= 37×10^4. The differences in the results for s= 0-1 were locally a few percent and for s= 1-2 up to 8%. In case the correction for the radiation was applied on our data, the difference for s= 0-1 increased up to 16 % and for s= 1-2 decreased to locally a few percent.

Igarashi did not mention any correction for radiation and used the higher turbulence level Tu= 0.5%, both these factors should give higher values on the upstream surface s= 0-1. For our data, the emissivity used in the correction for radiation may be somewhat overestimated (assumed = 1.0), giving possibly

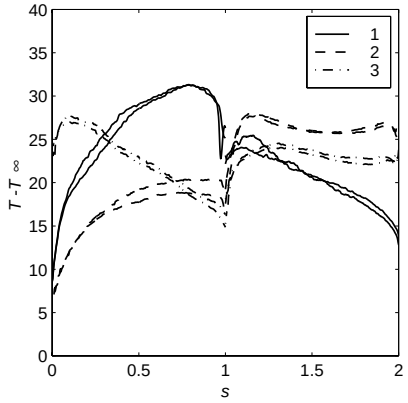

FIGURE 7. Measured sample surface temperatures on all four sides of the prism, for three configurations; 1. configuration A, single cylinder at $Re = 6.97 \times 10^4$, 2. configuration B, single prism with downstream plate at $Re = 7.48 \times 10^4$, 3. configuration C, the downstream prism of two arranged in-line at $p/D = 2.0$, at $Re = 3.75 \times 10^4$.

lower Nu along all surfaces. However, the relative effect on Nu of radiation is smaller for the higher Re investigated.

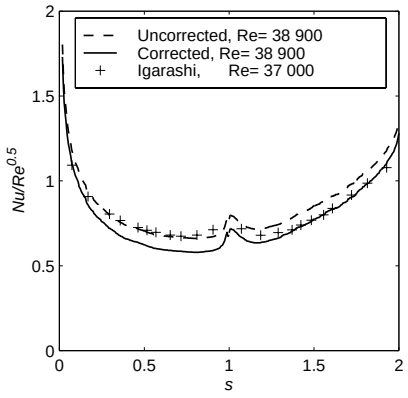

FIGURE 8. Comparison of our results for a singe prism (configuration A), corrected and uncorrected for radiation with those from Igarashi (1986).

The total error was calculated as the vector sum of the individual errors, which were assumed independent. The error in the local Nu was then estimated $\pm$ 8 %, (where the largest contribution was the TLC measured temperatures),

possible larger for lowest Re, and near the corners due to heat conduction in the insulation. The error in Re was estimated within $\pm$ 1%.

3.8. *Velocity measurements using PIV*

Velocity fields were obtained around the prisms using the PIV (particle Image Velocimetry) technique. Smoke particles of glycol were injected into the air flow, a laser sheet perpendicular to the prisms axis was then applied, using a 400 mJ double pulsed Md:Yag laser. The images of the smoke were captured, using the digital CCD camera Kodak ES 1.0, 1008×1018 pixels, cross correlations were performed one per second, on interrogation areas 32×32 pixels with 50% overlap to obtain the velocities. The camera to object distance was ca 1.5 m.

Qualitative conclusions were made on the flow pattern around the prisms based on observations from about 50 sample instantaneous velocity fields, for each geometry investigated.

4. Experimental results

4.1. *Single prism (configuration A)*

4.1.1. *The flow velocity fields*

Our measurements of the instantaneous velocity fields around a single prism at $\alpha = 45°$, are shown in Fig. 9 a and b. The flow separates from the corners and the shedding of vortices can be clearly seen downstream. Closer views of the near wake (within one side length from the prism surface) are shown in Fig. 10.

The magnitudes of the instantaneous velocities in the near wake were found similar to that of the free stream in front of the cylinder. From observations of the instantaneous velocity fields, three different flow patterns alternate periodically in the near wake: (1) flow crossing the prism horizontal symmetry line, and returning backwards along the surface, as seen in Fig. 10 a and d, (2) a calm wake and the main flow essentially bypassing the prism, as seen in Fig. 10 b, (3) backward directed flow not crossing the prism horizontal symmetry line, as seen in Fig. 10 c. Of these three patterns, (1) was observed to be the most frequent. The frequency of the alternation of these patterns is estimated to 40 Hertz, from the measurements of Strouhal numbers by Lee (1975). PIV measured velocity fields for a single prism at $\alpha = 45°$ are mot shown in the literature before as far is known.

4.1.2. *The convective heat transfer from the prism*

The Nusselt numbers (Nu) were measured over both the front and rear surfaces for a single prism at an attack angle of $\alpha = 45°$ (configuration A), and at Reynolds numbers in the range $3.89 \times 10^4 < Re < 1.05 \times 10^5$. The results are shown in Fig. 11 a. Nu increased with Re as expected, and the shape of the Nu vs. Re curves were similar for all Re.

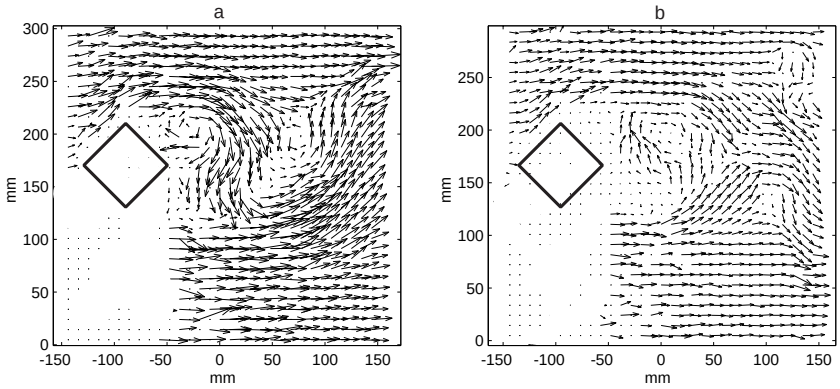

FIGURE 9. Instantaneous velocity data around a single prism at Re= 7.8×10^4, at instances a and b in time (Note: the left lower part of the flow field was not measured here, the laser light was shaded by the prism).

On the front upstream surfaces of the prism, Nu has a maximum at the upstream edge s= 0.00, from where it decreases sharply, asymptoting from about s=0.5 to a nearly constant value, and then from about s= 0.95 (just before the top corner) increasing sharply. The decrease is likely due to the increasing boundary layer thickness along the surface, and the subsequent increase due to increased velocity near the corner.

On the downstream surface, the average $\overline{Nu}_{1-2}$ was found to be higher, with a minimum at about s= 1.1 (where the corner effect abates), and maximum at the rear edge, s= 2.00. The decrease in Nu from $s = 2.0$ to $s = 1.0$, may be explained by the flow patterns in the near wake seen in Fig. 10 a and d, which indicates flow in average from $s = 2.0$ to $s = 1.0$ possibly with something like a boundary layer growth.

For the upstream surface, the average $\overline{Nu}_{0-1}$, was found to be correlated to Re by Eq. 5 and for the downstream surface, the average $\overline{Nu}_{1-2}$ by Eq. 6. The correlation exponent for the front surface (Eq. 5), e=0.52 (e= 0.48 when no correction for radiative heat flux was used in Eq. 1), compares well with e= 0.5 that is obtained from an analytical solution available for laminar flow over a 90° wedge (isothermal surface), Eckert (1942) . Since within the Re we used it is expected that the boundary layer is also laminar.

For the rear surface it was found that e= 0.75 (0.70 without correction for radiative heat flux), which is larger than e=0.67 found by Igarashi (1986). An uncertainty exist in the present correlation due to the stated error in Nu and the fact that the experiments were made for only three Re values.

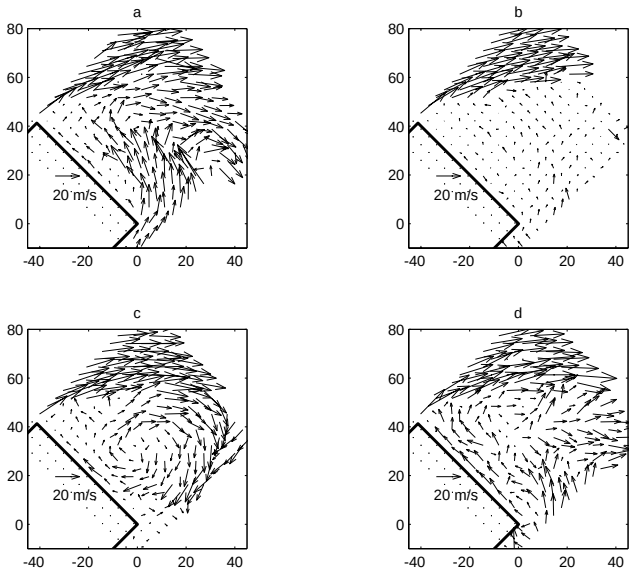

FIGURE 10. The instantaneous velocity field in the upper half of the near wake of a single prism at Re= $7.8{\times}10^4$, at instances a, b, c, and d in time.

$$Nu = 0.553 Re^{0.52} \tag{5}$$

$$Nu = 0.057 Re^{0.75} \tag{6}$$

4.2. *Single prism with a splitter plate (Fig. 6 configuration B)*

4.2.1. *The flow velocity fields*

In this configuration, a thin plate (2 mm thick) $5D$ long and as wide as the prism, was attached to the downstream of the prism along its centerline. Compared to a prism without the plate, this entirely changed the wake flow and significantly reduced the velocity fluctuations there. The instantaneous velocities seen in the wake, were found an order of magnitude lower than in the free stream , see Fig. 12 a and b. Limited regions of backward directed flow (of free stream magnitudes) in the wake, as can be seen in Fig. 12 b, did appear, but much less frequently. These infrequent occurrences of backward flow would have probably been eliminated if the plate was long enough to include the whole separated region of the wake.

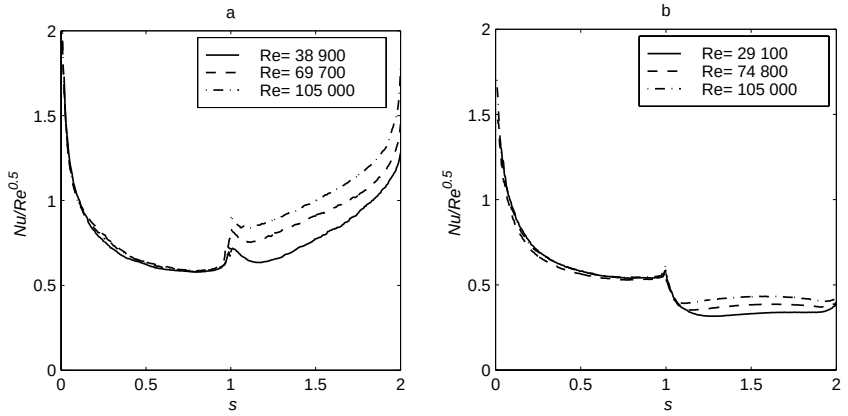

FIGURE 11. $Nu/Re^{0.5}$ at different Re along the surface of (a) a single prism (configuration A), (b) a prism with a downstream splitter plate (configuration B).

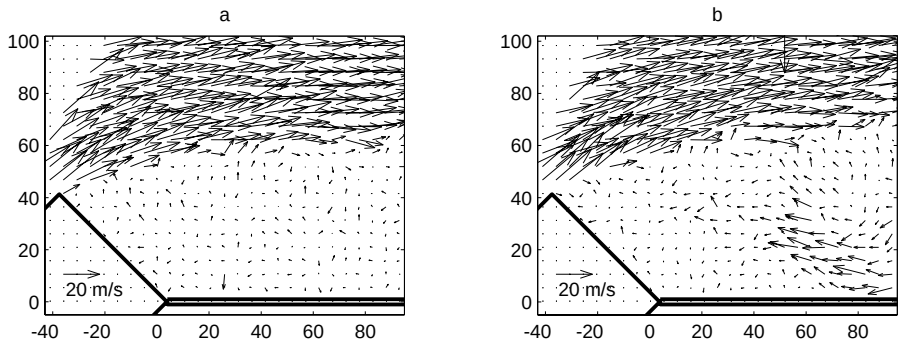

FIGURE 12. The measured instantaneous velocity field around a single prism with a downstream thin plate (Fig. 6 configuration B), $Re = 7.4 \times 10^4$ at instances a and b in time.

4.2.2. *The convective heat transfer*

At this configuration (B), Nu was measured for $29.1 \times 10^4 < Re < 1.05 \times 10^5$, and the results are shown in Fig. 11 b.

On the downstream surface, Nu was found significantly lower than on the upstream one ($\overline{Nu}_{1-2}$ was only 52 to 65 % of $\overline{Nu}_{0-1}$), and nearly constant. The uniformity is obviously a consequence of the uniform and low flow activity above the downstream prism surface, shown in Fig. 12 a and b.

Correlation of the average $\overline{Nu}_{0-1}$ with Re resulted in Eq. 7 for the upstream surface, and $\overline{Nu}_{1-2}$ in Eq. 8 for the downstream one.

$$\overline{Nu}_{0-1} = 0.667 Re^{0.496} \tag{7}$$

$$\overline{Nu}_{1-2} = 0.066 Re^{0.658} \tag{8}$$

Comparison of the heat transfer results for the single prism without and with the splitter plate (configurations A and B, respectively), is shown in Fig. 11 a and b. The magnitudes and trends on the upstream surface are similar in both configurations, but the average $\overline{Nu}_{0-1}$ along the upstream surface is 9% higher without the plate. The reason is not quite clear, one possibility is that the vortex shedding for the configuration without the plate may induce fluctuations also on the upstream surface.

For the prism without the plate, the average $\overline{Nu}_{1-2}$ (rear surface) was found for the highest Re to be 2.5 times higher than that for the prism with the plate. This observation is similar to that by Igarashi (1984*c*) for the separated region of a circular cylinder with and without a similar downstream plate.

4.3. *Two prisms positioned in-line, (Fig. 6 configuration C)*

4.3.1. *The velocity field for the pitch ratio $p/D = 1.45$*

Two prisms were positioned in-line with the upstream flow velocity direction (configuration C), and at the pitch (spacing) ratio of $p/D = 1.45$ their corners were nearly touching. The measured instantaneous velocity field between the prisms was measured and is shown in Fig. 13 a, b, c and d. The flow separates at the top corner $s = 1.0$ of the upstream prism, and the downstream prism is therefore located in its wake.

The flow near the surfaces and between the two prisms had velocities an order of magnitude lower than in the free stream. Backwards-directed flow over the downstream prism, of free stream velocity magnitudes, as can be seen in Fig. 13 a, c and d, was observed most of the time. No reattachment of flow was seen onto the downstream prism. This flow pattern is in agreement with observations by Igarashi (1981) (flow pattern A, shown in the Introduction here), made for two closely-spaced circular cylinders.

4.3.2. *The velocity field for the pitch ratio $p/D = 2.00$*

As shown in Fig. 14 a, b, c and d, the flow separates at the upstream prism, typically reattaching on the downstream prism, as is seen in Fig. 14 a, and d. Sometimes flow (of free stream velocity magnitude) crossed the horizontal symmetry centerline between the prisms, as can be seen in Fig. 14 c an d. This behavior agrees with that for two circular cylinders, shown by Igarashi (1981) (flow pattern B), which is shown in our Introduction.

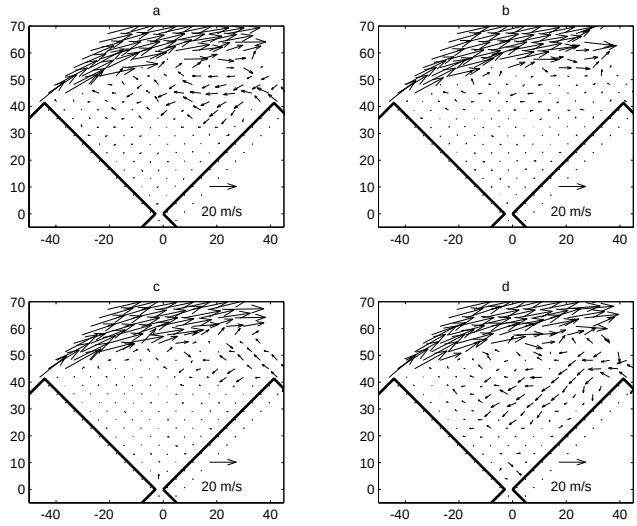

FIGURE 13. Instantaneous velocity data around two prisms $p/D = 1.45$ apart, $Re = 7.41 \times 10^4$, at instances a, b, c, and d in time.

The reattached flow created sometimes a vortex between the cylinders (of free stream velocity magnitude), as can be seen in Fig. 14 a. However, the backward directed flow over the downstream prism observed for the closer spacing $p/D = 1.45$, Fig. 13, did not appear here.

4.3.3. *The velocity field for the pitch ratio $p/D = 4.00$*

As shown in Fig. 15 a, b, c and d, the flow separates also for this pitch ratio at the upstream prism and reattaches on the downstream one (Fig. 15 a, c and d), creating vortices between the prisms, similar to the observation of citeIgarashi1981 (pattern C) for two in-line circular cylinders. Sometimes there was no reattachment, as shown in Fig. 15 b. Such by-pass flow was more frequent at this larger pitch ratio than for the smaller $p/D = 2.00$.

4.3.4. *Pitch ratios producing bi-stable flow*

It is noteworthy that for the pitch ratio in the range $5.83 < p/D < 6.67$, the flow was found to be unstable and intermittently switching over the two prisms, as indicated also by significant variations in the prism surface temperatures with time, and there were also clear time-variations in the flow-induced sound level from the prisms. The flow could be stable for some minutes, and then suddenly change, and again be stable in another pattern for some minutes. Experiments were performed for $p/D = 5.83$, 6.15, 6.42 and 6.67, only the pitch ratios $p/D = 5.83$ and 6.67 always produced stable flow during the test period of 25 minutes.

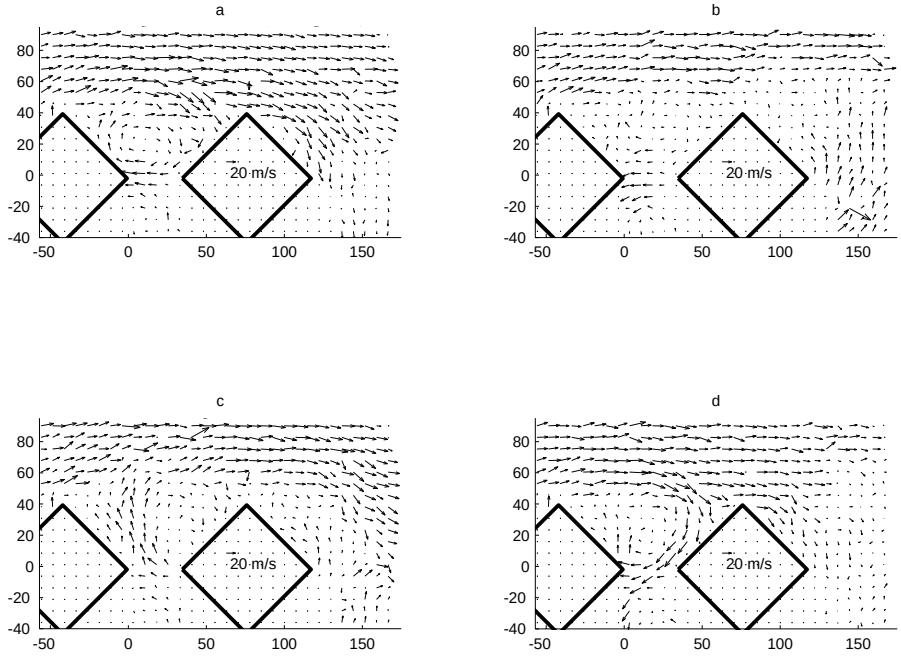

FIGURE 14. The instantaneous velocity field around two prisms p/D= 2.00 apart, Re= 7.2×10^4, for time instances a, b, c, and d.

Bi-stable flow were also observed by Igarashi (1981) for two in-line circular cylinders at $3.1 < p/d < 3.75$, where d is the diameter of the circular cylinder.

4.3.5. *The local $Nu/Re^{0.5}$ for the upstream prism*

The relations between the local surface values of the correlation parameter $Nu/Re^{0.5}$ and s, for the upstream of the two in-line prisms, for similar Re and for $1.45 \leq p/D \leq 8.00$, are shown in Fig. 16 a, b and c. For the upstream surface s= 0.00 to 1.00, $Nu/Re^{0.5}$ was found to be nearly independent of p/D.

On the downstream surface s=1.00 to 2.00, and for $p/D > 1.45$, $Nu/Re^{0.5}$ increases with s for all p/D in a qualitatively similar way, but its magnitudes differ. For comparison, $Nu/Re^{0.5}$ is also shown for a single prism (Fig. 11 configuration A), and is seen to be similar to that for p/D = 6.67 and 8.00, Fig. 16 c. This indicates independence from the downstream prism at these pitch ratios.

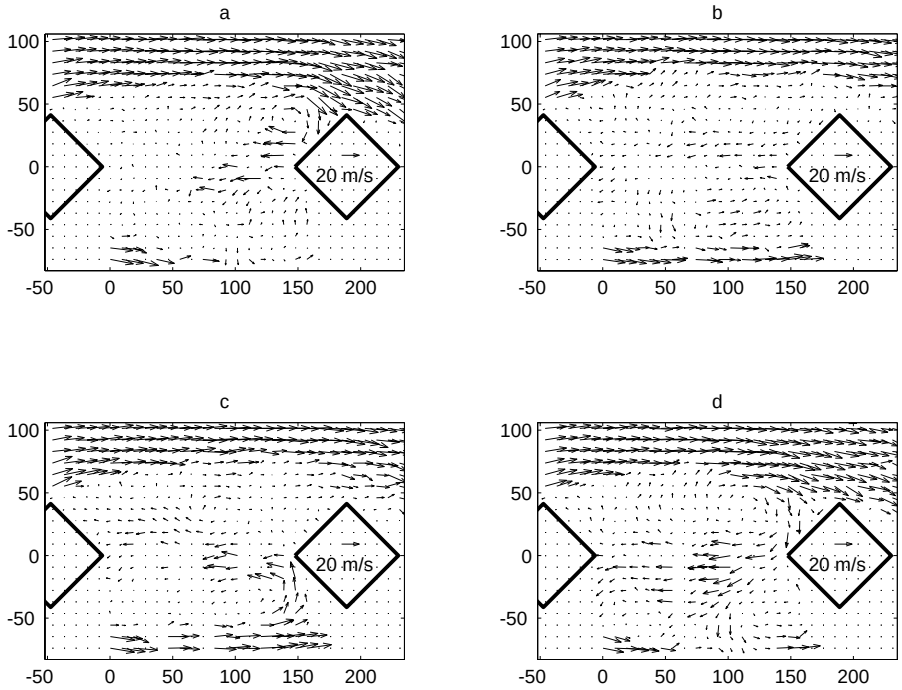

FIGURE 15. The instantaneous velocity field around two prisms p/D= 4.00 apart, Re= 7.04×10^4, for time instances a, b, c, and d.

4.3.6. *The local $Nu/Re^{0}.69$ for the downstream prism*

The relations between the local surface values of the correlation parameter $Nu/Re^{0.69}$ and s, for the downstream one of the two in-line prisms, for nearly-equal Re and for 1.45≤ p/D ≤6.67, are plotted in Fig. 17. Depending on the range of p/D, three different relationships can be discerned:

1) for $p/D \leq 1.5$, $Nu/Re^{0.69}$ basically gradually increased with s. This behavior could be explained by a flow from s= 2 over s= 1 and towards s= 0, seen in (Fig. 13).

2) for 1.66≤ p/D ≤5.83, Nu has a maximum at s= 1.00, decaying towards s= 0.00 and s= 2.00, probably due to the flow reattachment on to this prism in a region near s= 1.00, shown for p/D= 2.00 in Fig. 14 and for p/D= 4.00 in Fig. 15, giving a (turbulent) flow over both surfaces towards s= 2.00 and s= 0.00.

3) for p/D= 6.67, Nu drops with s from a maximum at s = 0.00, rises sharply to a second maximum at s = 1.00, then drops to a minimum at s= 1.1, from which it rises to the third maximum at s= 2.00. At this distance

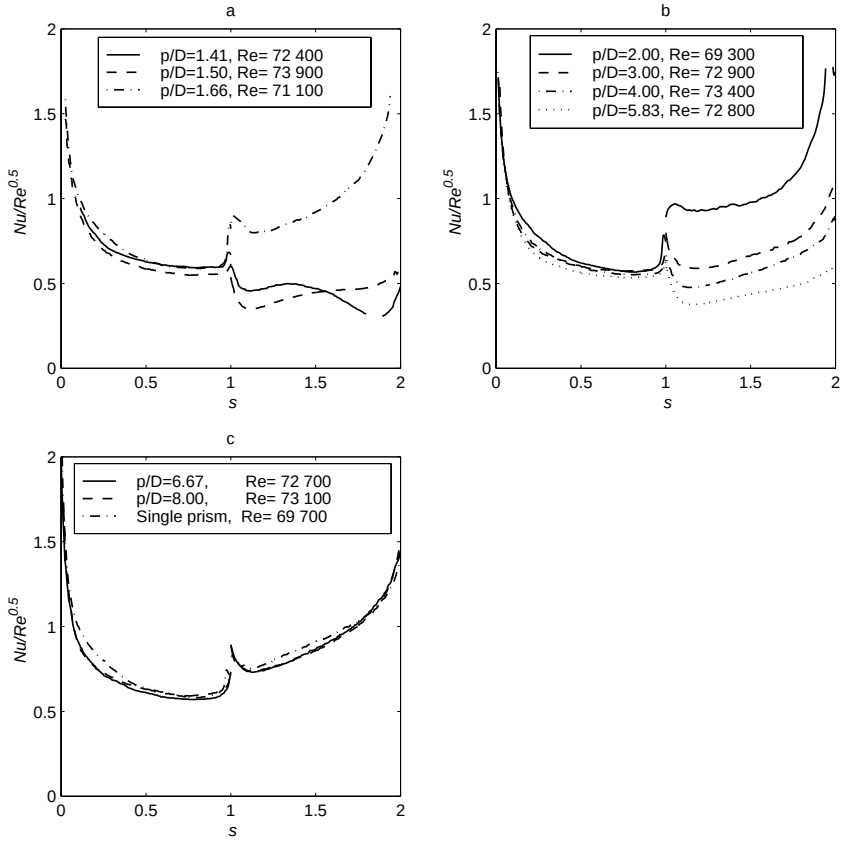

FIGURE 16. The relations between the local $Nu/Re^{0.5}$ and s, for the upstream prism of two in-line prisms, for different pitch ratios and at nearly-equal Re. a. for $p/D = 1.41$, 1.50, and 1.66, b. for $p/D = 2.00$. 3.00. 4.00, and 5.83, c. for $p/D =$ 6.67 and 8.00, and for a single prism (Fig. 11 a configuration A) for comparison.

relatively large p/D, the flow essentially flows onto the prism from its front, producing heat transfer fluxes qualitatively similar to those of a single prism in cross flow.

The relations between $Nu/Re^{0.69}$ and the surface position s, for the downstream prism at p/D= 1.5 was investigated for $2.3 \times 10^4 < Re < 1.39 \times 10^5$, and the results are shown in Fig. 18 a.

We correlated $\overline{Nu}_{0-1}$ with Re by Eq. 9, and the $\overline{Nu}_{1-2}$ by Eq. 10. The exponent e was found smaller for the front than for the rear surfaces, while for

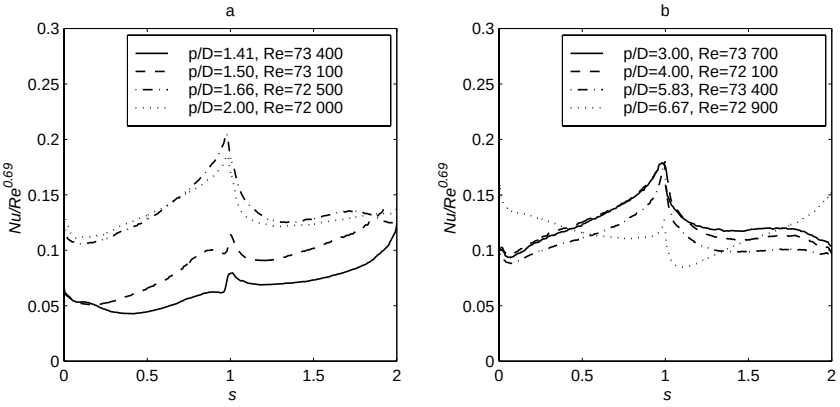

FIGURE 17. The relations between the local $Nu/Re^{0.69}$ and s, for the downstream prism of two in-line prisms, for different pitch ratios and at nearly-equal Re. a. for $p/D = 1.41$, 1.50, 1.66, and 2.00, b. for $p/D = 3.00$. 4.00, 5.83, and 6.67.

the average $\overline{Nu}_{0-2}$ e was found to be 0.69. Note that Nu had here a strong dependence on p/D, which may had some influence on the results.

$$\overline{Nu}_{0-1} = 0.14Re^{0.63} \tag{9}$$

$$\overline{Nu}_{1-2} = 0.07Re^{0.73} \tag{10}$$

The relations for p/D= 2.00 and $3.75 \times 10^4 < Re < 1.34 \times 10^5$ are shown in Fig. 18 b. The average $\overline{Nu}_{0-1}$ over the upstream surface was correlated to Re by Eq. 11, and the average $\overline{Nu}_{1-2}$ over the downstream surface by Eq. 12. The exponent e is fund to be nearly the same for the front and rear surfaces, and for the average $\overline{Nu}_{0-2}$ it was found to be 0.69.

$$\overline{Nu}_{0-1} = 0.148Re^{0.68} \tag{11}$$

$$\overline{Nu}_{1-2} = 0.117Re^{0.70} \tag{12}$$

Additional measurements were performed for p/D= 3.00 at $7.37 \times 10^4 < Re < 1.16 \times 10^5$, with the results shown in Fig. 18 c. The results indicate the same value of the exponent e for both surfaces as for that found for the shorter distance p/D= 2.00.

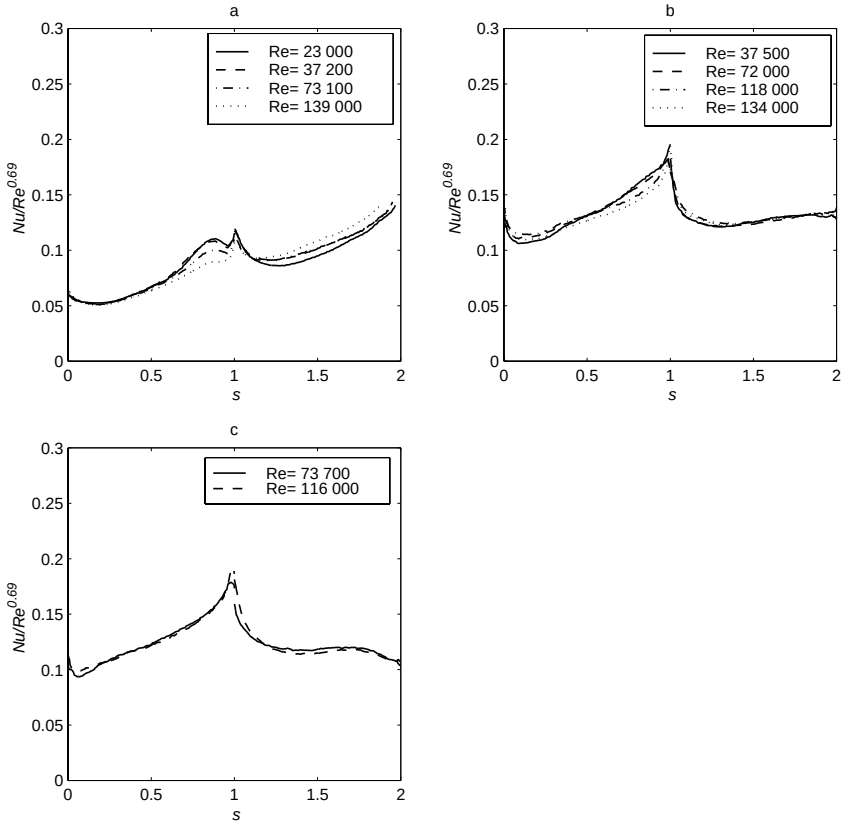

FIGURE 18. The relations between $Nu/Re^{0.69}$ and the surface position s, for the downstream prism of two in-line prisms, for different pitch ratios and Re. a. for p/D = 1.50, b. for p/D = 2.00, c. for p/D = 3.0.

4.4. *Group of four prisms, (Fig. 6, configuration D)*

The relations between the local $Nu/Re^{0.69}$ and s, for the downstream prism of four prisms mounted in a square pattern (Fig. 6, configuration D) for p/D= 2.50 and Re =3.48×10^4 and 8.88×10^4 are shown in Fig. 19. The relations were found to be qualitatively similar to those for the downstream prism of two in-line prisms at the largest distance investigated p/D= 6.67 (Fig. 17 b). In comparison to that case, Nu is higher on the upstream surface, and lower on the downstream surface.

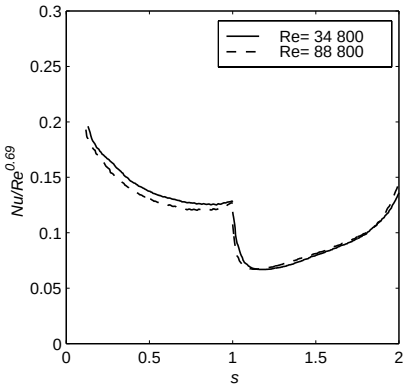

FIGURE 19. The relations between the local $Nu/Re^{0.69}$ and the surface position s, for the downstream prism of for the downstream prism of four prisms in a square (Fig. 6, configuration D), for p/D= 2.50 and different Reynolds numbers.

4.4.1. *Average values of Nu at the surfaces of the upstream prism*

The surface averages $\overline{Nu}_{0-1}$ and $\overline{Nu}_{1-2}$ were calculated for the upstream prism from the measured local values of Nu, for $6.93\times10^4 < Re < 7.39\times10^4$. As seen in Fig. 20 a, $\overline{Nu}_{0-1}$ was found to be almost constant for all pitch ratios $1.41< p/D <8.0$, and similar to that of a single prism, (infinite pitch ratio). A weak tendency to follow the changes in Nu on the downstream surface can be seen.

The variations in $\overline{Nu}_{1-2}$ with the pitch ratio (for the same, upstream prism) were larger, exhibiting two distinct minima and maxima. The first minimum occurs for p/D= 1.45, when the corners of the prisms were nearly touching, which is a consequence from the relatively small velocities of the fluctuating flow between the prisms, seen in Fig. 13.

The first maximum appears at the slightly higher spacing, of p/D= 2.0, which may be explained by the increase in velocities fluctuations as p/D increases (Fig. 14). For larger separations between the prisms there was a decay, and $\overline{Nu}_{1-2}$ was found to be halved at p/D= 5.83, where the second minimum occurs. This may be explained by the decreasing wake velocity fluctuations at this upstream prism, as seen by comparing the flows for p/D= 2.00 in Fig. 14 and for p/D= 4.00 in Fig. 15.

As was mentioned above, the flow for a range of larger separations between the prisms was found to be unstable, and convective heat transfer measurements were therefore not possible using the present technique, for which the flow needs to be stable at least five minutes to reach a steady state. For pitch ratios of p/D= 6.67 and larger, the flow was again stable, and $\overline{Nu}_{1-2}$ was almost double

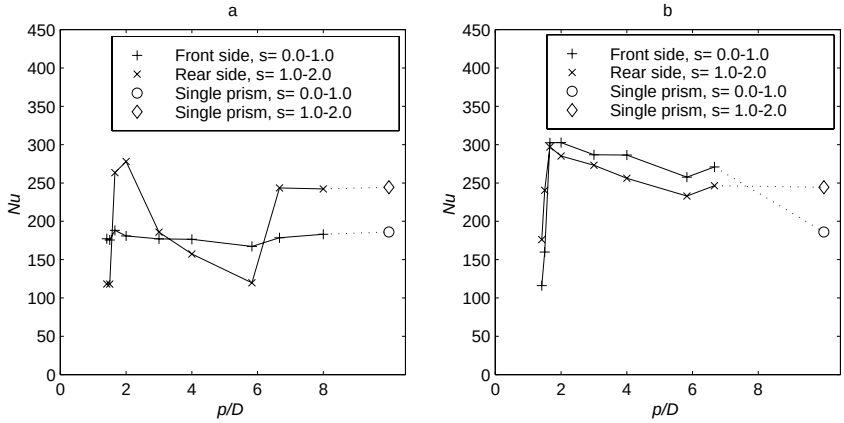

FIGURE 20. (a), the averages $\overline{Nu}_{0-1}$ and $\overline{Nu}_{1-2}$ for the upstream prism of two in-line prisms, for different distances between the prisms, and for $6.93\times10^4 < Re < 7.39\times10^4$. (The maximal effect of this variation in Re on $\overline{Nu}_{0-1}$ and $\overline{Nu}_{1-2}$ is 5%). (b) average $\overline{Nu}_{0-1}$ and $\overline{Nu}_{1-2}$ for the downstream prism, for $7.2\times10^4 < Re < 7.3\times10^4$. The results for a single prism (configuration A) is also shown.

compared to that at $p/D = 5.83$, and was further similar in magnitude to $\overline{Nu}_{1-2}$ for the downstream surface of a single prism, as shown in Fig. 20 a. Clearly, at the larger pitch ratios the flow around the upstream prisms was similar to the flow around a single prism.

4.4.2. *Average values of Nu at the surfaces of the downstream prism*

The surface averages $\overline{Nu}_{0-1}$ and $\overline{Nu}_{1-2}$ from the downstream prism, which is located in the wake of the first prism, are shown in Fig. 20 b. The magnitudes are similar on both sides of the prism since both of these two surfaces are in the wake region. A maximum and one less obvious minimum can be seen in the investigated pitch ratio interval. As expected, the lowest values appeared when the prisms were almost touching, at $p/D = 1.45$, but $\overline{Nu}_{1-2}$ (for the downstream (rear) surface) was found to be somewhat higher than $\overline{Nu}_{0-1}$ (for the upstream (front) surface). This difference can possibly be explained by the backward directed flow along the downstream surface, Fig. 13.

The magnitudes were doubled for $1.66 < p/D < 2.00$, which may be related to the reattachment of flow onto this prism, seen in Fig. 14. For larger distances between the two prisms there were a decay in $\overline{Nu}_{0-1}$ and $\overline{Nu}_{1-2}$, and both reached a minimum at $p/D = 5.83$, which may be explained by observations of

a number of the PIV measured flows, the number of flow reattachment events was estimated lower for p/D= 4.00, compared to p/D= 2.00.

At the larger distance p/D= 6.67, which was on the other side of the unstable flow region, both $\overline{Nu}_{0-1}$ and $\overline{Nu}_{1-2}$ was found somewhat higher. A large change appeared in the local Nu, which was shown in Fig. 17. $\overline{Nu}_{1-2}$ was found similar to that of a single prism, while $\overline{Nu}_{0-1}$ was found higher than a single prism. For further increased distances, $\overline{Nu}_{0-1}$ and $\overline{Nu}_{1-2}$ are expected to attain the same levels as for a single prism in cross flow, which also is shown for comparison.

5. Conclusions

Cross-flow convective heat transfer coefficient distribution for $2.9 \times 10^4 < Re < 1.39 \times 10^5$ was measured on single quadratic prisms with and without a downstream splitter plate, and on arrays of two and four prisms, all at the attack angle $\alpha = 45°$, and the associated velocity field was measured using particle image velocimetry. Physical insights were gained about the relationship between the heat transfer and the velocity fields.

For the single prism in cross flow investigated, there appeared vortex shedding in the wake as shown by the PIV measured velocities. Further, Nu was found similar to data measured by, Igarashi (1986). Some differences were found, which were related to the correction for radiation.

For the single prism in cross flow with a downstream plate, which reduced the vortex shedding, Nu was found on the upstream surface similar to Nu for a single prism, while Nu was found nearly constant and halved in magnitude along the downstream prism surface. The PIV measured velocity data confirmed the data by showing uniform and low velocity fluctuations in the near wake.

Two prisms were arranged in-line and Nu was measured on each of the two prisms within the range of pitch ratios $1.45 \leq p/D \leq 8.00$.

At the pitch ratio p/D= 1.45 the prisms edges were nearly touching and the flow showed no reattachment onto the downstream prism. The surface average $\overline{Nu}_{0-2}$ had in the range of pitch ratios minimum for both of the prisms .

At the larger distances between the two prisms $1.66 < p/D < 2.00$, a maximum in the average $\overline{Nu}_{0-2}$ appeared for both of the prisms. Explained by the PIV data, which showed reattachment of flow onto the downstream prism, which created large velocity fluctuations also in between the two prisms.

For the downstream prisms of the two prism in-line, and at the pitch ratio p/D= 2.00, the average $\overline{Nu}_{0-2}$ was found to be related to Re by,

$\overline{Nu}_{0-2} = 0.142Re^{0.69}$

The local Nu values showed qualitatively three different patterns on the down stream prism, for the pitch ratios $p/D \leq 1.5$, $1.66 \leq p/D \leq 5.83$, and $p/D \geq 6.67$.

The flow was found to be unstable (bi-stable) and intermittently switching over the two prisms, in the interval $5.83 < p/D < 6.67$.

6. Acknowledgments

This work was supported by AGA AB (now Linde Gas) and Ipsen International GmbH. Ulf Landen is acknowledged for his valuable help with the experimental equipment. We also want to thank Dr. Barbro M. Klingmann for her advice and comments.

References

Eckert, E. R. G. 1942 Die berechnung des wrmeuberganges in der laminaren grenschicht um strmter krper. *VDI-Forshungsheft* **416**, 1–24.

Igarashi, T. 1981 Characteristics of the flow around two circular cylinders arranged in tandem (1st report). *Bullentin of JSME* **24** (188), 323–331.

Igarashi, T. 1984*a* Characteristics of the flow around a square prism. *Bullentin of JSME* **27** (231), 1858–1865.

Igarashi, T. 1984*b* Characteristics of the flow around two circular cylinders arranged in tandem (2nd report, unique phenomenon at small spacing). *Bullentin of JSME* **27** (233), 2380–2387.

Igarashi, T. 1984*c* Correlation between heat transfer and fluctuating pressure in separated region of a circular prism. *Int. J. of Heat and Mass Transfer* **27** (6), 927–937.

Igarashi, T. 1985 Heat transfer from a square prism to an air stream. *Int. J. of Heat and Mass Transfer* **28** (1), 175–181.

Igarashi, T. 1986 Local heat transfer from a square prism to an air stream. *Int. J. of Heat and Mass Transfer* **29** (5), 777–784.

Lee, B. E. 1975 The effect of turbulence on the surface pressure field of a square prism. *J. Fluid Mech.* **69** (2), 263–282.

Lind, M., Lior, N., Alavyoon, F. & Bark, F. 1998 Flows effects and modeling in gas-cooled quenching. In *Proc. Heat Transfer 1998, 11th International Heat Transfer Conference, Kyongju, Korea*, , vol. 3, pp. 171–176.

Lindgren, B. & Johansson, A. V. 2002 Design and evaluation of a low-speed wind-tunnel with expanding corners. Technical report ISRNKTH/MEK/TR–02/14-SE. Dept. of mechanics, KTH.

Lior, N. 2003 The cooling process in gas quenching, invited keynote presentation and paper. In *Proc. International Conference on Advances in Materials and Processing Technology, AMPT 2003, Dublin, Ireland*, , vol. 1, pp. 171–179.

Ljungkrona, L., Norberg, C. & Sunden, B. 1991 Free-stream turbulence and tube spacing effects on surface pressure-fluctuations for 2 tubes in an in-line arrangement. *J. Fluid Struct* **5** (6), 701–727.

Roshko, A. 1955 On the wake and drag of bluff bodies. *J. of the aeronautical sciences* **22** (2), 124–132.

Roshko, A. 1993 Perspectives on bluff-body aerodynamics. *J. wind eng. ind. aerod.* **49 1-3**, 79–100.

Wiberg, R. & Lior, N. 2003 Error causes and magnitudes in thermochromic liquid crystals thermometry, paper imece2003-42101. In *IMECE'03, 2003 ASME International Mechanical Engineering Congress & Exposition Washington, D.C., USA*, pp. 15–21.

Zdravkovic, M. M., ed. 1997 *Flow around circular cylinders, vol. 1 Fundamentals*. Oxford science publications, Oxford University Press Inc.: Oxford.